CZECH TECHNICAL UNIVERSITY IN PRAGUE
Faculty of Nuclear Sciences and Physical Engineering
Department of Physical Electronics

Diploma Thesis

Software for tomographic reconstruction of refractive index profile of special optical fiber preforms

Author: Bc. Adam Novozámský
Supervisor: Ing. Jaroslav Pavel
Consultant: Ing. Pavel Peterka, Ph.D.
Academic year: 2009/2010

Herein I would like to thank my leaders Eng. Pavel Peterka, Ph.D. and Eng. Jaroslav Pavel for their expert guiding, my family for helping during my studies, and my God for his guiding in my live as well.

This work was supported by the Ministry of Education, Youth and Sports of the Czech Republic, Contract No. ME10119 „FILA“, and the Institutional research plan AV0Z20670512.

I declare that the submitted work was elaborated by me and I have mentioned all used documents and literature. And I am not aware that I violated any copyrights.

30th April 2010, Noviny pod Ralskem Adam Novozámský

Resume

Czech

Název práce:	Software pro tomografickou rekonstrukci profilu indexu lomu preforem speciálních optických vláken
Autor:	Bc. Adam Novozámský
Obor:	Inženýrská informatika
Druh práce:	Diplomová práce
Vedoucí práce:	Ing. Jaroslav Pavel, Katedra fyzikální elektroniky, Fakulta jaderná a fyzikálně inženýrská, České vysoké učení technické v Praze
Konzultant:	Ing. Pavel Peterka, Ph.D., Ústav fotoniky a elektroniky, Akademie věd České republiky

Abstrakt: Cílem práce je seznámení se s optickými vláknovými zesilovači a lasery, s měřením indexu lomu na přístroji A2600 a následné vytvoření počítačového programu pro tomografickou rekonstrukci profilu indexu lomu preforem optických vláken. Vstupem programu budou deflekční funkce naměřené pro určitou preformu analyzátorem preforem Photon Kinetics A2600. Spolehlivost tomografického výpočtu bude ověřena nejprve na teoretických deflekčních funkcích preforem se známým profilem indexu lomu a posléze na měření kruhově symetrických preforem. Analýza profilu indexu lomu kruhově nesymetrických preforem bude ukázána na výsledcích tomografické rekonstrukce profilu indexu lomu preformy pro dvouplášťová vlákna, určené pro pláštěm čerpané vláknové zesilovače.

Klíčová slova: optické vlákno, optický zesilovač, laser, tomografie, MatLab

English

Title:	Software for tomographic reconstruction of refractive index profile of special optical fiber preforms
Author:	Bc. Adam Novozámský
Branch:	Engineering informatics
Type of work:	Diploma thesis
Labor Leader:	Eng. Jaroslav Pavel, Department of Physical Electronics, Faculty of Nuclear Sciences and Physical Engineering, Czech Technical University in Prague
Consultant:	Eng. Pavel Peterka, Ph.D., Institute of Photonics and Electronics, Academy of Sciences of the Czech Republic
Abstract:	The aims of this work is getting familiar with optical fiber amplifiers and lasers, with measurement of the refractive index profile at the device A2600 and then make a computer program for tomographic reconstruction of refractive index profile of optical fiber preforms. The input to the program will be deflection function measured for a certain preform with the preform analyzer Photon Kinetics A2600. Reliability of tomography calculation will first be tested on the theoretical deflection function of preform with known refractive index of profile, and then for measuring circularly symmetrical preform. Analysis of the refractive index profile circularly asymmetric preforms will be shown on the results of tomographic reconstruction of the refractive index profile of preforms for double-clad fiber, designed for cladding pumped fiber amplifier.
Key words:	optical fiber, optical amplifier, laser, tomography, MatLab

Contents

List of Figures

List of Tables

Writing Conventions

We used the special text conventions for better understanding of the project documentation. These text conventions are described in the following [Table 1].

Table 1 - Document Conventions

Description	Meaning	Example
Italic Times-Roman	Some comments or names	*Comment.*
Times-Roman in square brackets	Reference to other chapters	[3.2.1.1]
	Reference to the figure, table, or equation	[Figure 3]
Bold Consolas superscript in square brackets	Referenced document	`[D1]`
	Referenced www	`[W1]`
	Referenced software	`[S1]`
Plain Consolas	Code or button in software	`main()`

In this document we used some images, which is in the **GNU Free Documentation License** or **Public Domain** because its copyright has expired (It has been more than 70 years after the death of the author.):

GNU Free Documentation License:	**[G]**
Public Domain:	**[PD]**

Unless otherwise stated, I am the author of the picture.

If the reference document is typed in a chapter title, the whole chapter is partial inspired by this referenced document.

1 Preface

This project is part of my course of master's studies at the Department of Physical Electronics at the Faculty of Nuclear Sciences and Physical Engineering, at the Czech Technical University in Prague. My study program "Information Technologies" offers a complex education in programming and knowledge of electronics. Last year I attended the subject Optoelectronics, that contained also several lab-tours in The Institute of Photonics and Electronics (IPE). IPE is a medium-size non-profit research institution belonging to the Academy of Sciences of the Czech Republic, the Czech largest non-university research organization. Here I met a lot of interesting projects and established contacts that led also to my thesis. The Institute of Photonics and Electronics is my taskmaster.

The subject of my thesis is the software in MATLAB for tomographic reconstruction of refractive index profile of special optical fiber preforms. This is an experimental characterization of preforms prepared in the laboratory at the Department of Optical Fibers Technology of the IPE. In this department, special optical fibers are prepared for basic research of fiber lasers and amplifiers, and last but not least optical fiber sensors. They are using MCVD – Modified Chemical Vapor Deposition [4.2.5.1] for the preforms preparation.

Conclusive parameter which determinates the waveguide properties of optical fibers is their refractive index profile. These Preforms have the same refractive index profile as the fibers produced from them. The fiber is basically our preform transformed to a smaller diameter.

From the knowledge of the refractive index profile in preforms, we can obtain much information about the fibers. We can estimate and count the diameter and numerical aperture, the cross-section shape, in case of a circular preforms we can appoint the core concentricity and the other properties (the cutoff wavelength, chromatic dispersion). Without this knowledge, we are not able to give the feedback for the technological procedure by the preform producing.

It is really necessary to correctly analyze the refractive index of the preform. At the Department of Optical Fibers Technology we measure the profile with analyzer Photon Kinetics A2600. We need to analyze circular and non-circular symmetric preform, because fiber amplifiers or fiber sensors developed in IPE sometimes has not circular symmetric refractive index profile. Therefore we need to develop own tomographic software for reconstruction of refractive index profile. And it is the goal of this thesis.

Former employee of the Institute of Photonics and Electronics, Ing. Jiří Slánička, worked on this work before me. He wrote several scripts in MATLAB, but he was unable to follow through the end this application. Therefore, our work derives in part from him. The main responsibility is to incorporate his script to our algorithm, whole tomographic visualization, and a final compilation of the program.

Our degree program of Information Technology is also taught comprehensive education course of optoelectronics and the conjugation of programming, analyzes and optoelectronic was the main reason, why I choose this issue. The promise of routine use of my developed application in scientific work was another big motivation.

2 Task

Topic:

Software for tomographic reconstruction of refractive index profile of special optical fiber preform

Elaboration instructions:

I. Get acquainted with fiber amplifiers and lasers
II. Learn how to measure the refractive index profile of preform with analyzer PK A2600
III. Devise and debug a program for visualization refractive index preform

3 Introduction

This chapter provides a historical overview of the development of fiber optic communications, some basic fundamental principles, and a comparison of copper and optical fiber technologies. It is just a brief introduction and not a comprehensive statement.

3.1 Something from Historical Note [W2]

In recent years it has become apparent that fiber-optics are steadily replacing copper wire as an appropriate means of communication signal transmission. They span the long distances between local phone systems as well as providing the backbone for many network systems. Other system users include cable television services, university campuses, office buildings, industrial plants, and electric utility companies. Optics has gone the way of several centuries to get to the level of today's optical fiber.

Here are some basic milestones in this long development chronology stacked:

Table 2 - Historical Overview

Beginnings	From the beginning people used fires to the transmission of signals between distant places. A Greek historian, mathematician, and scholar Polybius (ca. 203–120 BC) developed a method of sending characters. Now we call it *Polybius Square* [Table 3]. Each letter is indicated by a show of two sets of torches. One set of fires represented rows of the matrix and the other set represented the columns of the matrix.
984	Although the first who described the law of refraction was Muslim scientist Abū ʿAlī al-Ḥasan ibn al-Ḥasan ibn al-Haytham (Alhazen), we usually call it the Snell's law, because Snell Willebrord rediscovered this law in 1621.

Table 3 - Polybius Square

	1	**2**	**3**	**4**	**5**
1	**A**	**B**	**C**	**D**	**E**
2	**F**	**G**	**H**	**I/J**	**K**
3	**L**	**M**	**N**	**O**	**P**
4	**Q**	**R**	**S**	**T**	**U**
5	**V**	**W**	**X**	**Y**	**Z**

The original *Polybius square* used the Greek alphabet.

Equation 1

$$n_1 \sin\theta_1 = n_2 \sin\theta_2$$

1665 Francesco Maria Grimaldi was the first who described and characterized the effects of diffraction of light. He also derived the term diffraction from the Latin – *diffringere* (=to break into pieces), referring to light breaking up into different directions. His results of observations were published posthumously in this year.

1670-1672 During this period, Newton lectured optics and he examined the refraction of light. He showed that a prism could decompose white light into a spectrum of colors and attributed these effects of diffraction to inflexion of light rays.

He also found out that the coloured light does not change its properties by separating out a coloured beam and shining it on various objects. He concluded from this that the color is the result of interaction with objects and not objects that create the color yourself. This is known as Newton's theory of colour.

1792 French engineer Claude Chappe developed and demonstrate the first optical telegraph system using semaphores that eventually spanned all of France.

Messages were relayed from one hill to the next using moving semaphore arms. This machinery was the first practical telecommunications system of the industrial age.

Figure 1 - Chappe's Optical Telegraph [PD]

1800 On February 11th 1800, A Hanoverian astronomer and composer Sir Frederick William Herschel was testing filters for the observing the sun spots with his telescope. In his experiments he discovered that a certain part of the spectrum of light contained infrared energy.

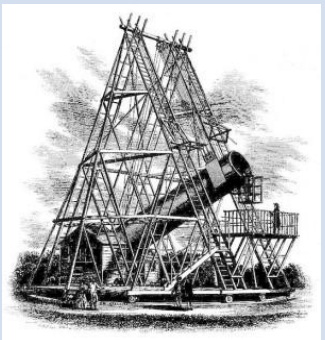

Figure 2 - Herschel's 12m Telescope [PD]

1803 Thomas Young performed a great experiment demonstrating interference in the context of light as a wave on two closely spaced slits. From his many achievements the most important was to establish the wave theory of light.

1815 French mathematician Augustine Fresnel came out form the finding of Thomas Young and he assumed that light is constructed of sinusoidal waves. He designed the first mathematical model to explain the properties of light.

1841 Swiss professor Daniel Colladon described the transmission of light down through a beam of falling water via total internal reflection of the light. The so-called "Colladon's fountain" is historically significant event today because it demonstrates the foundation for modern fiber optic technology.

1864 Scottish theoretical physicist and mathematician James Clerk Maxwell laid the foundations for the study of light transmission in the form of electromagnetic waves. Maxwell's set of equations demonstrated that electricity, magnetism and even light are all manifestations of the same phenomenon: the electromagnetic field.

1880 Alexander Bell invented a device called Photophone. The idea of the photophone was thus to modulate a light beam that was shining on it via sound and vibrating mirror. As the sound quivered the mirror, its modulated beam of light and reflect this light to a distant location. For the demodulation of the reflected light he used crystalline selenium cells at the focal point of its parabolic receiver. Applying this method, Bell was able to communicate to a maximum distance of 213 meters.

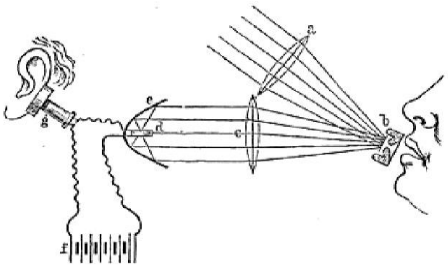

Figure 3 - Bells Photophone Schema [PD]

1907 British experimenter H. J. Round observed the electroluminescence in 1907 by the using a crystal of silicon carbide and a cat's-whisker detector.

1910 Hondros and Debye showed via integration of Maxwell's equations that in dielectric wires can spread electromagnetic waves too. However, these waves are different significantly from the waves of conductive wires. They found that arise only when oscillating period does not exceed certain limits depending on the dielectric constant of the substance and the wire radius. Furthermore, they found out that the wave with the maximum possible period is spreading across the wire with the speed of light and electric field lines is almost perpendicular to the surface of the wire.

1917	Einstein theorized that the energy in each quantum of light was equal to the frequency multiplied by a constant, later called Planck's constant. He deduced it from Max Planck's law of radiation. He published this idea in the paper: *Zur Quantentheorie der Strahlung* (On the Quantum Theory of Radiation).
1927	Russian scientist and inventor Losev published details in a Russian journal of the first-ever light emitting diode (LED).
1927	The first image transmission through tubes was demonstrated independently by the radio experimenter Clarence Hansell and the television pioneer and engineer John Logie Baird.
1934	An American engineer Norman R. French first patented the idea of optical telephone system. He described how speech signals could be transmitted via down a thin piece of glass. The appoint used cable has to be make out of solid glass or a similar material with a low attenuation coefficient at the operating wavelength. Unfortunately, there were no transparent materials available with sufficiently low attenuation, at that time.
1956	In this year Brian O'Brien, in the United States, and Harry Hopkins and Narinder Singh Kapany, in England, found the way to guide the light. Their concept was making a two-layer fiber. Inner layer called the core the other layer called the cladding. The term 'fiber optics' was first used by Kapany.
1960	An American physicist Theodore Harold Maiman demonstrated the first functional laser at the Hughes Research Laboratories. Great pioneering work on the development of LASER and MASER did two Soviet physicists Alexander Mikhaylovich Prokhorov and Nicolay Gennadiyevich Basov and American Charles Hard Townes. They shared the 1964 Nobel Prize in Physics.
1966	A pioneer in the development and use of fiber optics in telecommunications Charles Kuen Kao concluded that the fundamental limitation for glass light attenuation is below 20dB/km, which is a key threshold value for optical communications. The results were first presented in January 1966 in London by Kao, and further published in July with his former colleague George Hockham. This conclusion opened the intense race to find low-loss materials and suitable fibers for reaching such criteria. In the

	following years developed Kao and his team important techniques and configurations for glass fiber waveguides.
1970	The researchers Robert D. Maurer, Donald Keck, Peter C. Schultz, and Frank Zimar in Corning Glass Works company (now Corning Incorporated) developed a technique for manufacturing glass fibers that exhibited the attenuation below 20dB/km. They achieve this result with fiber by doping silica glass with titanium.
1972	The same team reduced signal attenuation in optical fibers to 4 dB/km using germanium dioxide as the core dopant.
1973	Low-loss silica fiber was used to make diode-laser-pumped fiber laser.
1976	This year, the company Rediffusion (a British business which distributed radio and TV signals) experimented in Hastings with its local cable operations and installed the first commercial fiber optic system for transmission of analog television signals. So fiber optic communication systems became commercially available.
1987	The Erbium-doped fiber amplifiers (EDFA) were first demonstrated by a group from the University of Southampton and a group from AT&T Bell Labs.
1991	The emerging field of photonic crystals led to the development of photonic-crystal fiber (PCF) which guides light by means of diffraction from a periodic structure.
2000	The first photonic crystal fibers became commercially available.

If you are interested in more detailed chronological history of fiber optics, we recommend you to visit Jeff Hecht's web page [W3].

3.2 Fundamental Principals

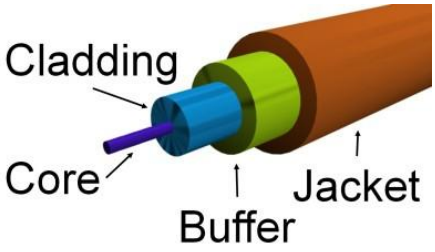

Figure 4 - The Structure of a Typical Fiber

An optical fiber is a glass or plastic fiber that carries light along its length. Fiber optics is an overlap of applied science and engineering concerned with the design and application of optical fibers. They are widely used in communications or illumination. Specially designed fibers are used for a variety of other applications, including sensors and fiber lasers.

An optical fiber is a cylindrical dielectric waveguide that transmits light along its axis. They have a very simple structure. The part which provides the light guidance consists of two sections: the glass or plastic core and the cladding layer. Both are made of dielectric materials – core is usually SiO_2 doped with Ge or P (diameter 2 - 50 μm); cladding is usually clear SiO_2 (diameter 125 μm; 250 μm). In practice, the cladding is usually coated with a tough resin buffer layer (usually named Coating), and for better features may be further surrounded by a jacket layer, usually polymer. These protective layers add strength to the fiber but do not contribute to its optical wave guide properties. The Buffer we denote as the primary protection and the jacket secondary. The cable can be very flexible, but traditional fiber's loss increases greatly if the fiber is bent with a radius smaller than around 30 mm. With this curve begins to emit a beam outside the cable. More expensive cables are still reinforced between the Buffer and Jacket layers with Aramid strength member – a class of heat-resistant and strong synthetic microfibers.

The basics of light propagation can be discussed with the use of geometric optics. The mechanism of light guidance is described in Snell's law [Equation 1] and a graphical representation we see in [Figure 5.a].

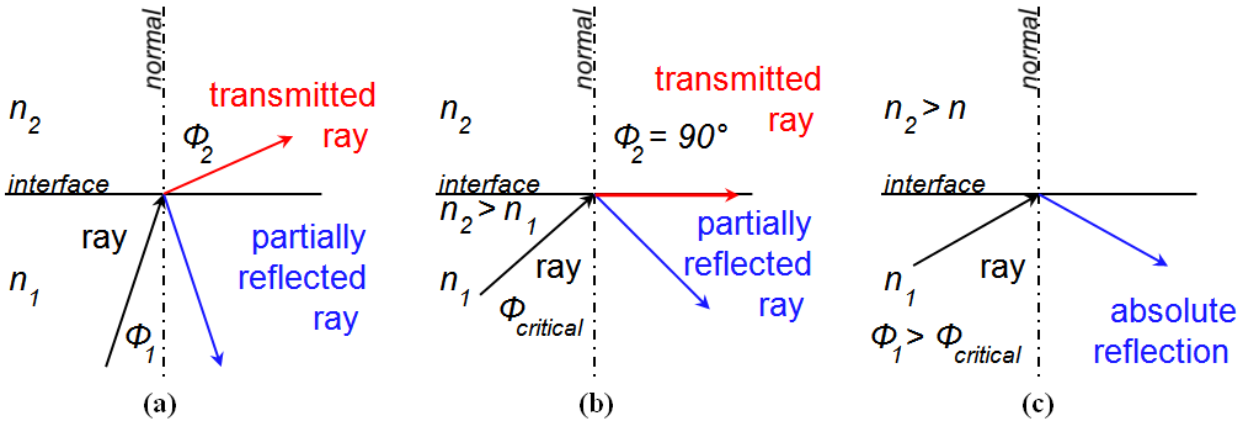

Figure 5 - Snell's Law

The index of refraction (n_1 and n_2 in the figure) is calculated by dividing the speed of light in a vacuum ($\approx 3 \cdot 10^8 m/s$) by the speed of light in some other medium. By definition it is clear that the index of refraction of a vacuum is therefore 1. As we can see in [Figure 5.b], to confine the optical signal in the core, the refractive index of the core must be greater than that of the cladding.

When the light is flying in core, it will be completely reflected from a boundary due to the larger than the "critical angle" [Figure 5.c] given for the boundary. This effect is used to confine light in the core. The critical angle we can count easily from Snell's Law, where we substitute the value of 90° for θ_2. Based on this, we can say that only light that enters the fiber within a certain range of angles can be transmitted by fiber without leaking out. This range of angles is called the acceptance cone of the fiber. This cone is derived by rotating the acceptance angle about the fiber axis [Figure 6].

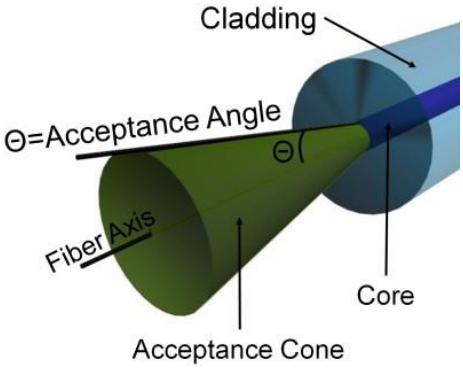

Figure 6 - Acceptance Cone

The sine of this acceptance angle (or maximum angle) is the numerical aperture (NA) of the fiber. Waveguides with a larger NA requires less precision to splice and work with than fiber with a smaller NA.

Equation 2

$$\sin\theta = \sqrt{n_1^2 - n_2^2} = NA$$

Equation 3

$$\sin\theta = \sqrt{n_1^2(0) - n_2^2} = NA$$

There are three types of fiber optic cable commonly used:

- multimode with step-index profile (SI) [Figure 7.a]
- "Gradient" fiber with a parabolic profile (graded index: GI) [Figure 7.b]; [Equation 3]
- single mode [Figure 7.c]

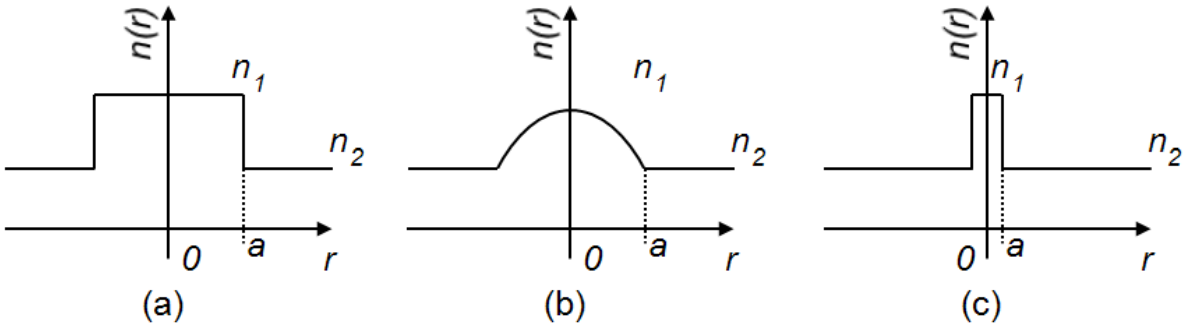

Figure 7 - Fiber Types: refractive index profile

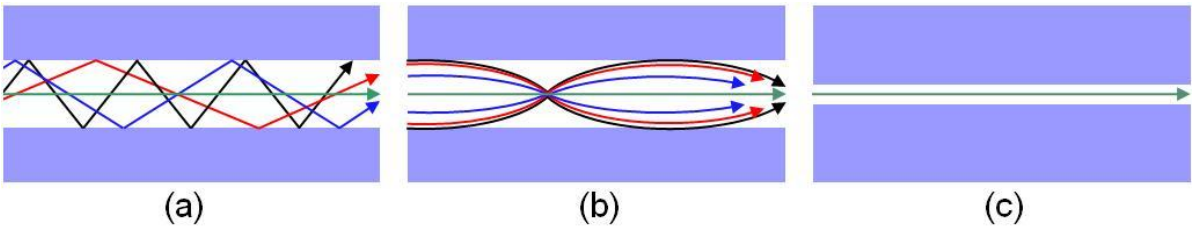

Figure 8 - Spreading Rays in Optical Fiber

3.2.1 SI Multimode Fiber

Multi-mode fiber is best suited for communication over shorter distances, such as those used in Local Area Networks (LANs) and Storage Area Networks (SANs). It has a large core, up to 100 microns *(A micron is one millionth of a meter.)* in diameter. Most common are the two standard widths, 62.5 micron and 50 micron. The first one fiber can support 10GbE *(10 Gigabit Ethernet)* over distances as long as 275 meters, the second, 50 micron multi-mode fiber, can increase that range to 550 meters. It has usually a cladding diameter of 125 μm. Passage of the beam by SI multimode fiber we can see in [Figure 8.a].

3.2.2 GI Multimode Fiber

A graded-index or gradient-index fiber contains a core in which the refractive index diminishes gradually from the center axis out toward the cladding. The higher refractive index at the center makes the light rays moving down the axis advance more slowly than those near the cladding. Light rays follow sinusoidal paths in the core of the fiber. The advantage of the graded-index fiber compared to multimode step-index fiber is the considerable decrease in modal dispersion. Modal dispersion is a distortion mechanism occurring in multimode waveguides, where the signal is spread in time because the propagation velocity of the optical signal is not the same for all modes. Passage of the beam by GI multimode fiber we can see in [Figure 8.b].

3.2.3 Single-Mode Fiber

Single-mode fiber is a type of fiber optic cable through which only one light signal can travel at a time. It has a narrow core - a typical single mode optical fiber has a core diameter between 8 and 10 μm and a cladding diameter of 125 μm. The big advantage of this type of waveguide is absence of modal dispersion. The index of refraction between the core and the cladding changes less than it does for multimode fibers. It leads also to the very small NA and necessity of more precision to splice. Equipment for single mode fiber is more expensive

than equipment for multi-mode optical fiber, but transmission using this waveguide does not suffer from modal dispersion. Passage of the beam by SM fiber we can see in [Figure 8.c].

3.3 Advantages and Disadvantages of Optical Fiber

Fiber optics are replacing traditional wire transmission lines, such as twisted pair, coaxial cable and microwave wave guides, for most telecommunications applications that are longer than a few hundred meters. In the 80th years, as this new technology reducing costs in production and overall reduced prices, fiber optic links were extended to major buildings and industrial and educational campuses. Now in the 21st century fiber optics is being extended to the home. The main reasons for this expansion we found in benefits described below.

The Advantages of Fiber over Wire Include:

- Large data-carrying capacity
- Low loss of signal; repeater-less transmission over long distances is possible
- High bandwidth
- Non-conductive, non-inductive
- Noise immunity; no affected by electromagnetic or radio frequency interference – potential for lower bit error rates can increase circuit efficiency
- No radiate electromagnetic pulses, radiation, or other energy that can be detected – difficult to eavesdrop on the line, providing better physical network security
- No crosstalk between cables
- Small size and low weight
- High electrical resistance; safe to use near high-voltage equipment or between areas with different earth potentials
- Signals contain very little power
- No sparks or heat
- Wide temperature range – temperatures from -40°C to +100°C; the record is 537°C
- Stable performance – affected less by moisture: less corrosion and degradation
- Material availability – silica glass is readily available
- Lower cost in the long run

The Few Disadvantages:

- High investment cost – individual components may be relatively expensive
- More expensive optical transmitters and receivers

- More difficult and expensive splicing
- Cannot carry electrical power to operate terminal devices

Almost all these disadvantages have been surmounted or bypassed in contemporary telecommunications usage. Nowadays communication systems are now unthinkable without fiber optics. Their operational expenditures is much more economic and effective than old wires.

4 Fiber Amplifiers and Lasers

4.1 Introduction to Lasers

The term "LASER" is an acronym for "Light Amplification by Stimulated Emission of Radiation", coined in 1957 by the laser pioneer Gordon Gould. It is an electronic-optical device that emits coherent light radiation. Although this original meaning meant a principle of operation, the term is now mostly used for devices generating light based on the laser principle.

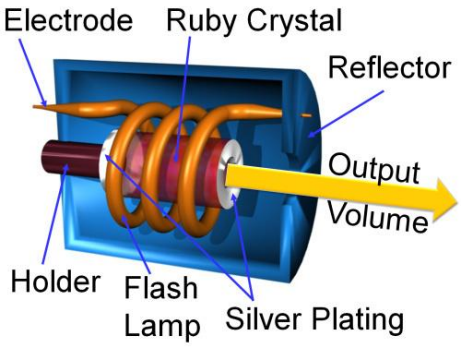

Figure 9 - Ruby Laser

The first working laser device was demonstrated on May 16, 1960 by Theodore Harold Maiman at Hughes Research Laboratories. Here Maiman presented a pulsed ruby laser [Figure 9]. His work was based on theoretical work on the operation principles of lasers, and a microwave amplifier and oscillator (MASER), which developed Nikolay Basov, Alexander Prokhorov, and Charles Hard Townes's group in 1953. Soon after the discovery of the laser were made the first gas laser (a helium–neon laser) and the first laser diode.

Laser beam has a number of very special properties:

- It can propagate over long lengths without much divergence
- It can be focused to very small spots
- It can have a very narrow bandwidth (most other light sources emit light with a very broad spectrum)
- It may be emitted continuously or in the form of short or ultra-short pulses, with durations from microseconds down to a few femtoseconds

For all these reasons, the laser technology is at the core of the wider area of photonics.

4.1.1 Basic Principle of Laser

A laser usually consists of an optical resonator in which light can circulate. It could be laser resonator, a highly reflective optical cavity or in its simplest form a set of two mirrors. Typically one of the two mirrors, the output coupler, is partially transparent. The output laser beam is emitted through this mirror. Within this resonator is situated a gain medium (e.g. a

laser crystal), which is a material with properties that allow it to amplify light by stimulated emission. Without the gain medium, the circulating light would become weaker and weaker in each resonator round trip. The gain medium of a laser is a material of controlled purity, size, concentration, and shape, which amplifies the beam by the process of stimulated emission. It can be of any state: gas, liquid, solid or plasma. The gain medium requires some external supply of energy. The process of supplying the energy required for the amplification is called "pumping".

There are more options for energy supply:

- ***Optical pumping:*** light of a specific wavelength that passes through the gain medium is absorbed.
- ***Electrical pumping***: an electric current (e.g., in semiconductor lasers).

The gain medium absorbs pump energy, which raises some electrons into higher-energy quantum states. We called these electrons - excited electrons. Particles can interact with light both by absorbing photons and by emitting photons. Emission can be spontaneous or stimulated. In the latter case, the photon is emitted in the same direction as the incoming photon. When the number of particles in one excited state exceeds the number of particles in some lower-energy state, population inversion is achieved and the amount of stimulated emission due to light that passes through is larger than the amount of absorption. Hence, the light is amplified. By itself, this makes an optical amplifier.

The light generated by stimulated emission is very similar to the input signal in terms of wavelength, phase, and polarization. This gives laser light its characteristic coherence, and allows it to maintain the uniform polarization and often monochromaticity established by the optical cavity design. [W5]

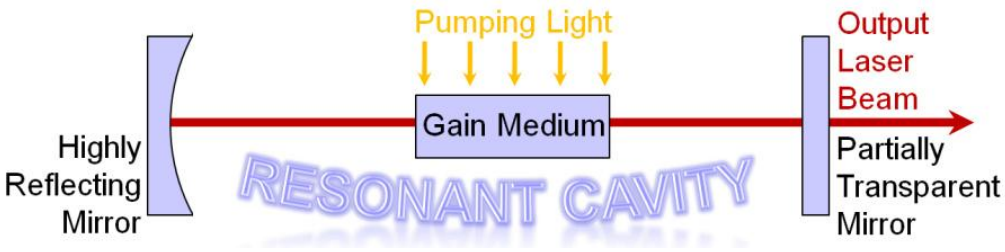

Figure 10 - Setup of a Simple Optically Pumped Laser

A laser cannot operate if the gain is smaller than the resonator losses, but if the gain is larger than the losses, the power of the light in the laser resonator quickly rises.

4.2 Fiber Lasers and Amplifiers

The first-generation fiber amplifier was developed by Elias Snitzer at the American Optical Company in 1964, just after the first functional laser was invented and demonstrated by Theodore Harold Maiman. In this early experiment, a signal from an injection laser diode was amplified in Neodymium (Nd^{3+}) doped fiber. Neodymium ion doped fiber was excited by a linear flash lamp. This Laser generated coherent radiation volume at a wavelength of 1.06 μm. The fiber had a core of 10 μm with a 0.75 to 1.5 mm cladding, a length of 1 m and with active environment wrapped in a spiral around the lamp, which performs the function of optical pumping. [Figure 11] shows the components used in the l964 experiment. The refractive index of core was 1.531 and the cladding had 1.51.

Although the active ion was efficient, the pumping scheme (flash lamp) was not efficient because its fluorescence spectrum was too wide for the narrow absorption spectrum of Neodymium ions. In addition, the host multi-component glass fiber was not a low loss medium. Consequently, high gain amplification was not achieved.

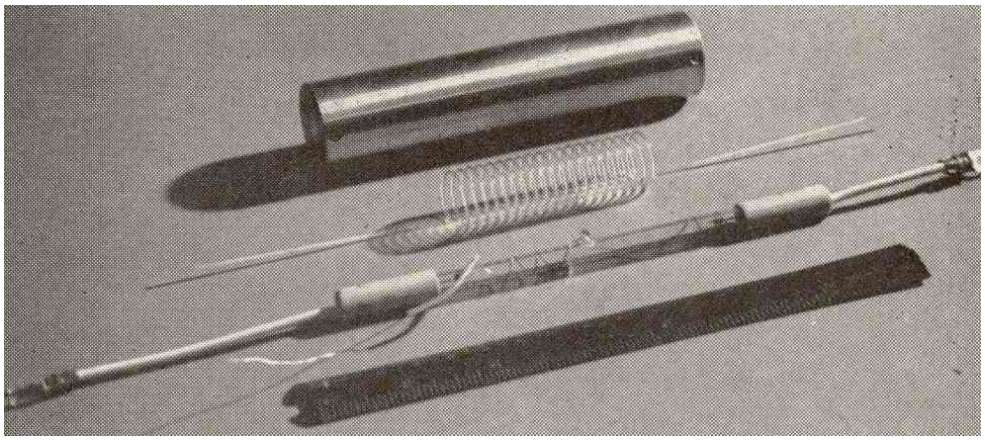

Figure 11 - Components of Coiled Fiber Laser [D3]

Despite the rampant development of solid-state laser in the coming years, fiber lasers have fallen into oblivion. Against the development and progress in the field of fiber optics, they stay rather a laboratory curiosity. The main reason was their poor performance, because in the 60 and 70 of the last century were not yet available powerful semiconductor diode pumping.

The breakthrough came in 1987, when a group from Southampton University led by David N. Payn reported high gain fiber amplifiers which they achieve by using Erbium-doped silica-based fibers.

This group had made great improvements, especially in terms of pumping scheme and host fiber. They recognized that Erbium (Er^{3+}) ion was ideally suited as an amplifying medium for modern fiber-optic transmission systems, due to its propitious transition at 1.5 μm.

Furthermore they replaced flash lamp with Ar^+ - pumped laser operating at 0.65μm as a pumping source. And finally they also used a low-loss and high numerical aperture host fiber, which was prepared based on the modified chemical vapor deposition (MCVD) method, which is an excellent technique for preparing low loss high silica fibers for optical fiber transmission. About this method we discussed in a separate chapter [4.2.5.1].

The principle of fiber laser uses the idea that light at one wavelength as the energy source can amplify light at a second wavelength. If a laser-active atom or ion is in an excited state, it may after some time spontaneously decay into a lower energy level, releasing energy in the form of a photon, emitted in a random spatial direction. This process is called ***spontaneous emission*** [Figure 12.a].

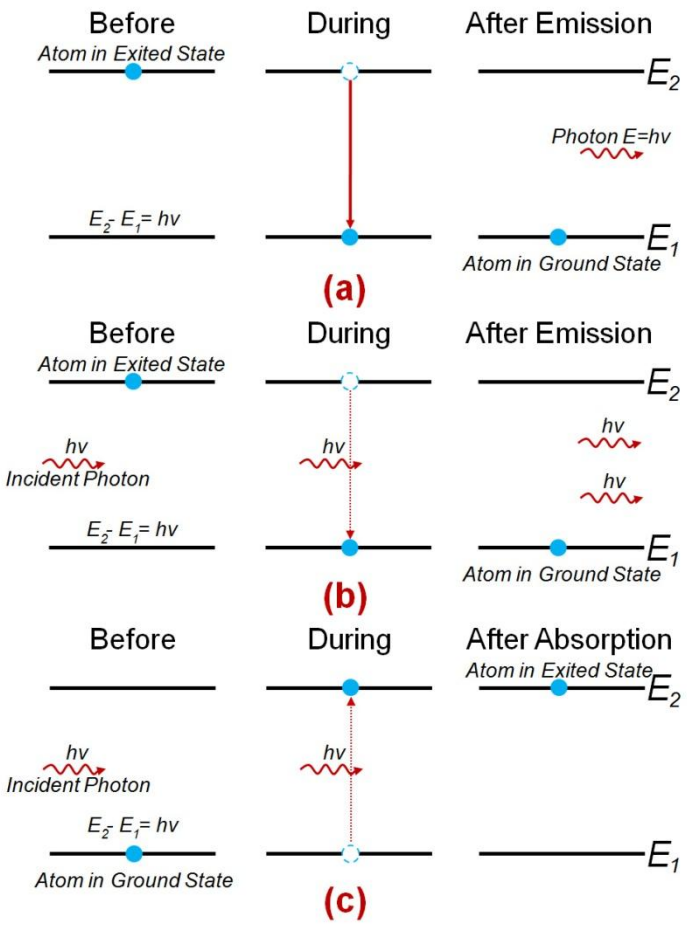

Figure 12 - Transitions between Levels

However, we can induce also the photon emission by incoming photons, if these have suitable photon energy (depends on their optical frequency:$E = h\nu$). This is called ***stimulated emission*** [Figure 12.b]. In that case, a photon is emitted into the mode of the incoming photon; this means that the newly generated photon has the same phase, frequency, polarization, and direction of travel as the original. In effect, the power of the incoming radiation is amplified. This is the physical basis of light amplification in laser amplifiers and laser oscillators.

If the environment gets photon energy equal to the difference in energy levels and the atom was in ground state, the photon can be absorbed and the atom can get into the excited state. This phenomenon is called ***absorption*** [Figure 12.c].

Under the conditions of thermal equilibrium given by the Boltzmann distribution [Equation 4] the lower energy level E_1 of the two-level atomic system contains most of the atoms.

Equation 4

$$\frac{N_1}{N_2} = \frac{g_1 e^{-E_1/KT}}{g_2 e^{-E_2/KT}} = \frac{g_1}{g_2} e^{(E_2-E_2)/KT} = \frac{g_1}{g_2} e^{h\nu/KT}$$

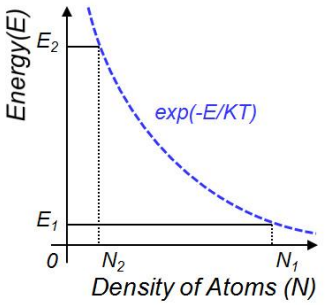

Figure 13 - Boltzmann Distribution of Atoms

This situation is illustrated in Figure [Figure 13] - it is normal for structures at room temperature. However, to achieve optical amplification it is necessary to create non-equilibrium distribution of atoms such that the population of the upper energy level is greater than that of the lower energy level ($N_2 > N_1$). This condition is known as population inversion. This process is achieved using an external energy source: our already well-known ***pumping***, when atoms are excited into the higher energy state through stimulated absorption. If the pumping source of radiation is so strong that the number of electrons in excited state outweighs the number of electrons in the basic state, environment begins to amplify the input signal.

4.2.1 Erbium Doped Fiber Amplifier [D4]

There are many different rare-earth ions, such as neodymium or ytterbium, which can be used to make fiber amplifier or laser capable of operating over a wide wavelength range extending from 0.4 to 4 μm, but we will focus on erbium.

Erbium is a chemical element with the symbol Er and atomic number 68 belonging to the group of rare earth metals. Erbium-doped glasses can be used as optical amplification media. The core of this special fiber is doped with erbium, which acts as a storage medium for the transfer of energy from pump to signal. The most common pump scheme is illustrated in [Figure 14] - the various levels are marked by Russell Saunders convention, based on the quantum theory of atoms. The pumping light at a wavelength of 980 nm is absorbed by the erbium ions. This absorption excites them to a higher energy level, $^4I_{11/2}$. The ions on this level rapidly disintegrate to a long-lived metastable state, $^4I_{13/2}$ (in-band pumping $^4I_{15/2} \rightarrow {}^4I_{13/2}$ at 1.48 μm is also possible).

Subsequent amplification is based on a simple principle; input (amplified) photon interacts with atoms in the excited state. It could occur spontaneous emission, but the lifetime of this metastable state in silica is typically 8-10 ms, so it is much more probable that emission will be stimulated by a traveling signal

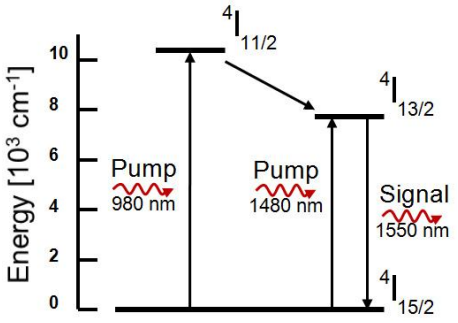

Figure 14 - Energy Bands

around 1.55 μm. This wavelength is especially important for optical communications because standard single mode optical fibers have minimal loss at this particular wavelength. If there is a spontaneous emission, the signal is amplified and contributes to the overall noise of amplifier.

A possible schema of a simple EDFA *(Erbium Doped Fiber Amplifier)* is in [Figure 15].

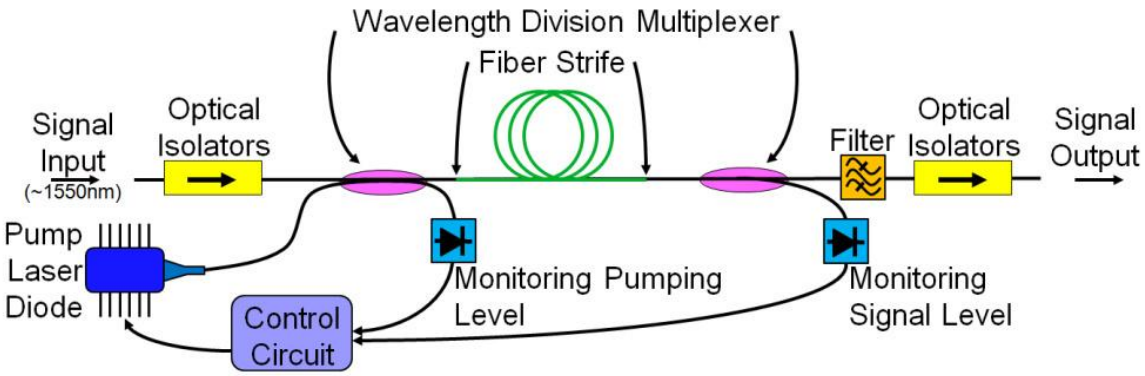

Figure 15 - Schematic Diagram of EDFA

Erbium doped fiber (length from meters to tens of meters) is welded with a transmission fiber. The first wave selective coupler (WDM - Wavelength Division Multiplexer) combines the light for pumping with the light of signal. The second WDM, behind the fiber, compensates for any unabsorbed pumping. Pump laser diode has a wavelength of 980 or 1480 nm. Pass filter suppresses noise from spontaneous emission and optical isolator eliminates unwanted reflections. An optical isolator is an optical component which allows the transmission of light in only one direction, using *Faraday Effect* (the main component is the Faraday rotator). Optoelectronic feedback loop governs the gain of amplifiers and pumping power.

EDFAs are used in optical communications to regenerate signals subdued absorption and scattering in the transmission fiber. We insert them into the long-distance transmission lines after about 70-100 km of optical cable, or use them as low-noise preamplifier to improve receiver sensitivity. As we have mentioned before, the development and the progress of optical fiber amplifiers have provided new and exciting improvements for optical fiber systems.

Some Advantages of EDFA [W5]:

- Transparent to bit rates and transmission formats.
- Simultaneous amplification of a large number of channel wavelengths.
- The gain of rare earth doped fiber amplifiers is insensitive to polarization - active dipoles are randomly oriented in the glass matrix.

- The gain is stable over 100°C temperature range due to homogeneous line broadening.
- Due to a relatively long upper level lifetime (10ms), the gain is "almost" immune to interference between light channels.
- Noise figure close to theoretical limit of 3dB can be achieved.
- Rare earth doped fiber amplifiers are compatible with transmission fibers and other fiber components.

The fiber attenuation is no longer limiting characteristic and expensive regenerator stations can be eliminated.

4.2.2 Continuous Wave Fiber Lasers

We can understand lasers as optical oscillators with a variety of choices for the laser cavity. The most common type is known as the Fabry-Perot cavity *(Fabry-Perot resonator = FPR)*, which is made by placing the gain medium between two high-reflecting mirrors [Figure 16]. In most cases of fiber lasers, mirrors are coupled to the fiber ends. This idea was first applied in practice in 1964 for a Nd-doped fiber. For this experiment have been used mirrors with high reflectance at wavelength 1.088 μm, and at the same time, highly permeable at the pump wavelength of 0.82 μm. The big problem was with diffraction losses, because they rapidly increased only at a slight tilt of fiber or mirrors - tolerable tilts were less than 1°.

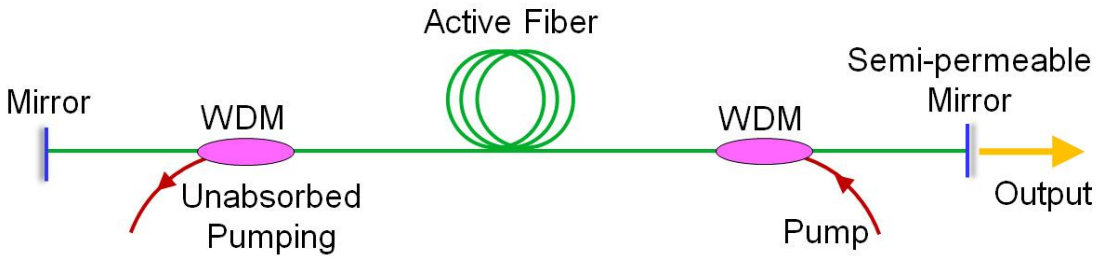

Figure 16 - Fiber Laser: Fabry-Perot Resonator

Possible solution to this problem is deposition dielectric coatings directly onto the polished ends of a doped fiber. However, the great sensitivity to imperfections at the fiber tip lingers. Furthermore, dielectric coatings can be easily damaged when high-power pump light is coupled into the fiber.

Figure 17 - Fiber Laser with Bragg Gratings

One of the several alternatives is to use a fiber Bragg grating (FBG), which acts as a high-reflectivity mirror for the laser wavelength while being transparent to pump radiation [Figure 17]. FBG is a periodic or aperiodic perturbation of the effective refractive index in the core of an optical fiber. Typical FBGs have grating periods of a few hundred nanometers. Grid FBG is produced by illumination of fiber with an external UV laser through the phase mask, such as microscopic grid etched in quartz back plate. The final interference pattern of high power ultraviolet radiation creates along the illuminated fiber a periodic modulation of refractive index that interrupts a molecular link in the core doped with germanium. The periodic grating will reflect light with a wavelength which is in resonance with the lattice period. All other wavelengths will leak. Bragg gratings are commonly used in optical networks as a selective wave filters. FBG compared with ordinary mirrors maintain the advantage of radiation propagation in optical fibers. It means that the pumping and laser output is thus possible to lead again through optical fibers.

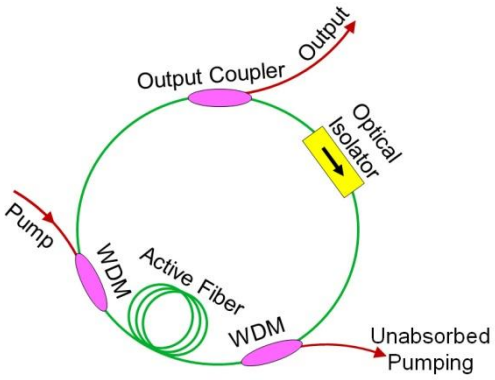

Figure 18 - Schema of Ring Laser

Another solution can take advantage of fiber couplers, which are called ***wavelength-division multiplexing*** (**WDM**) couplers. WDM is a method of combining multiple signals on laser beams where optical signals with different wavelengths are combined, transmitted together, and separated again. They are design such that most of the unabsorbed pump power comes out of the port that is a part of the laser cavity.

Ring Fiber Laser

A ring cavity was used as early as 1985 by creation an Nd-doped fiber laser. Since then, several new designs have emerged. In the [Figure 18], there is a one of the typical and simple arrangement of the fiber-loop laser, when the output of the amplifier is brought to the entrance – it thus created a ring-resonator. A similar scheme is often used to realize unidirectional operation of a laser. An advantage is that a ring cavity can be made without using mirrors. The circular resonator *(Ring Fiber Laser)* includes also the output fiber coupler for pulling the laser signal out. An isolator is also inserted within the loop for unidirectional operation – it provides generation of laser signal in one direction, and contributes to the stability of the output signal.

If no signal is at the input of fiber amplifier, the feedback signal is equal to zero and there is no output signal. Such a situation is unstable. Slightest noise (with frequency components falling within the frequency band amplifier), which exists due to spontaneous emission necessarily always, can initiate an oscillation on input. The input signal is amplified and output is led back to the entrance and then again and again amplified. This process repeats until the signal is not so large that further enlargement of the signal is limited by reducing the gain amplifiers (saturation). Steady state is achieved when the amplifier gain exactly compensates the loss of a feedback loop in one circulation loop.

Another condition of steady, stationary oscillations is the phase synchronism: the total change of the phase in one runaround must be an integer multiple of 2π, so the signal feedback is phased with the original input signal. This condition is fulfilled for a wide range of optical waves and modes spreading in the resonator. In the case of FPR are these so-called longitudinal modes separated by a distance on the frequency $\Delta\nu = \hat{c}/2d$, where $\hat{c}$ is the speed of light in fiber (about $2 \times 10^8\, m/s$) and d is the length of the resonator. The optical wave passes through an optical fiber in FPR twice, but in the laser passes through the ring just once. Therefore, the modes are separated by a distance on the frequency $\Delta\nu = \hat{c}/d$. It is clear that the Ring Laser must be twice as long as the FPR if we want the same frequency distances modes.

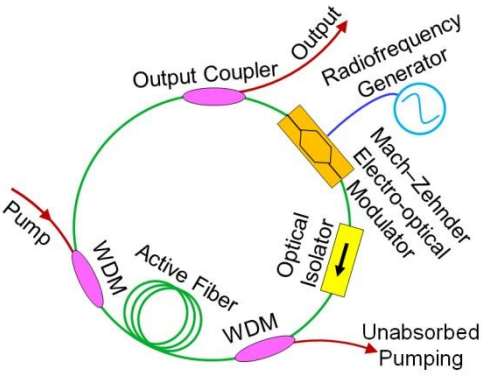

Figure 19 - Pulsed Fiber Laser with an Active Mode Sync

Pulsed Fiber Lasers

Within the spectral band amplification of erbium may fit hundreds of thousands of longitudinal modes; line width transition Er^{3+} is about 30 nm, respectively 4 THz. These modes typically oscillate independently of each other – regime of freely oscillating modes. However, there are methods to achieve mutual binding and phase-coincidence of modes, called mode synchronization. We can see each mode as the Fourier components of the expansion of periodic function with period $T = 1/\Delta\nu$, which is equal to the time of one circulation of light waves in resonator. This periodic function represents a sequence of optical pulses. Time pulse width is inversely proportional to the number of longitudinal modes, and hence bandwidth transition. System of synchronization modes can be achieved by inserting an optical modulator into the laser cavity, which opens periodically with period T. The modulator can be controlled by an external frequency generator; so-called ***active mode***

locking. In [Figure 19] assume this function the *Mach-Zehnder amplitude modulator*, which is created from a crystal of lithium niobate ($LiNBO_3$).

We can also use passive closure consisting of saturable absorbing environment; so-called ***passive mode locking***. Such closure may be e.g. polarizer in combination with non-linear swivelling polarization in the optical fiber of resonator, as shown in [Figure 20]. For the activities closure is essential nonlinear propagation of light in fiber. Light travels through the core fiber, which has a diameter of about 8 microns. The average light intensity in the core overtop the light intensity on the surface of the Sun by the performance of about 1 W and the peak intensity of the pulses may be higher order. Here we can watch the phenomenon known as Kerr-effect dependence of the refractive index of glass on the intensity. This change in refractive index significantly influences changes in pulse shape and polarization of the spreading, because is different in different parts of the pulse.

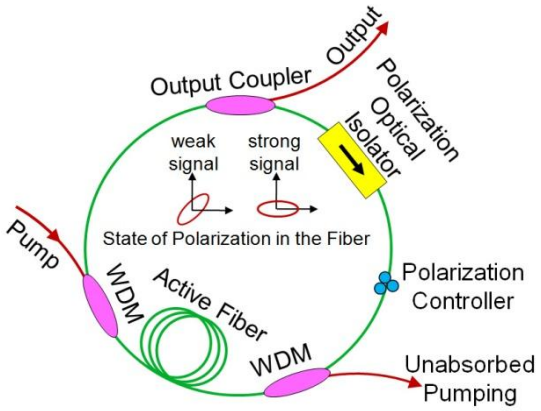

Figure 20 - Pulsed Fiber Laser with a Passive Mode Sync

We set the polarization of light waves due to ***polarization controller*** so that the weak signal is perpendicular to the polarization axis of polarizer's bandwidth, but the wave is twisted by an intensity so that it pass through polarization optical isolator with small losses. Nonlinear spreading in fiber is also involved in forming the shape of pulses, e.g. a phase auto-modulation can lead to pulses compression.

The group of nonlinear fiber optics at the Institute of Photonics and Electronics deal among other things to a study of pulse fiber lasers. There were developed passive by mode locked fiber lasers with repeating frequency in the order of units to tens of MHz; active by mode locked fiber lasers with repeating frequency in the order of hundreds of MHz to GHz units; and fiber lasers based on modulation instability with repeating frequency of several hundred GHz. These lasers based on modulation instability may be an attractive source of optical pulses for future communication systems with high transmission speed. In these lasers is achieved a phase synchronization in quad-wave mixing via cross modulation and self-phase modulation. As an active environment was used optical fiber doped by erbium and ytterbium. Pumping radiation does not excite directly the erbium ions, but the energy is absorbed by pumping ytterbium ions, which transfer energy to erbium ions. These lasers operate at a wavelength 1550 nm and for pumping are used ytterbium fiber laser or Nd: YAG-laser.

4.2.3 Methods for Pumping of Active Fibers

The pumping of active fiber can be done in many different ways. The first way was pumping with flash lamp from the side of fiber. It was used also in the Elias Snitzer's fiber laser [Figure 11]. This method was very inefficient. Another and widely dispersed way is to installation the pumping directly to the core of active fiber. This method requires elements that guarantee the separation of amplified signal and pumping signal. The disadvantage is the need for single-mode pumping beam, which brings problems of effective establishment of radiation laser diode into the fiber, and last but not least the expensiveness of single mode diode.

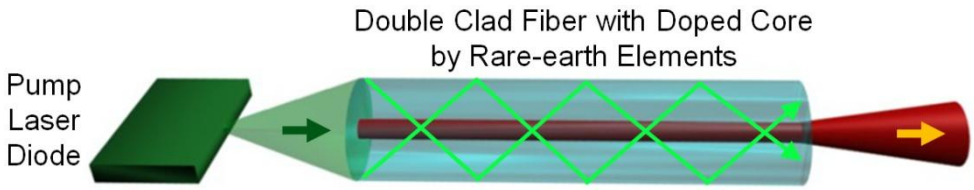

Figure 21 - Principle of Double Clad Laser

Another approach to increasing output power of fiber lasers came at end of the eighties, when it was discovered the method for pumping an active environment through the cladding. In this way it is possible to transform a highly divergent volume of multimode laser diodes with a large radiating surface into the good-quality single mode laser beam with low divergence. Discoverer of the method – called ***double clad*** – was again Elias Snitzer, author of the idea first fiber laser. Principle of laser double clad active fiber is shown in [Figure 21].

This design is called double clad given that there are two guiding structures, the core and the glass cladding surrounding the core. The core (indicated in red in [Figure 22]) is doped by erbium or other rare earth elements capable of laser amplification. The glass inner cladding (indicated in light-blue) has a lower refractive index than the core and is surrounded by lower index polysiloxane polymer outer second cladding which allows it to become a guiding structure. The core of the waveguide serves for a signal and is usually single mode. Pump light is launched from the fiber end into the undoped inner cladding, propagating in a multimode fashion and interacting with the doped core as it travels along the fiber, schematically shown in green in [Figure 21]. Since the inner cladding has a

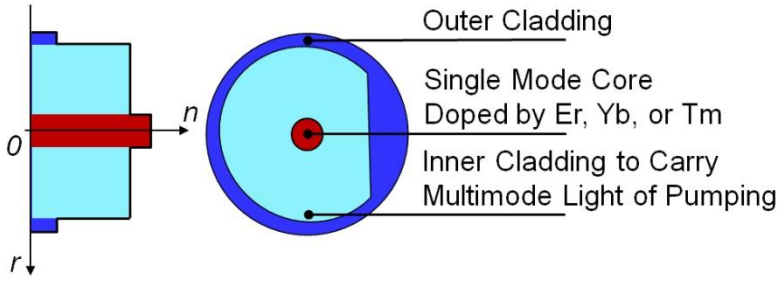

Figure 22 - Double Clad Fiber

relatively large cross-sectional area, it is possible to couple into it a large amount of optical power using the pump laser diode. As the pump radiation is traveling along the fiber, again and again is crossing the area of the doped core, and is absorbed by the rare-earth ions. These excited ions can then devolve their energy on the amplified signal by the stimulated emission. They are compact, have small dimensions, and excellent quality of mode output volume thanks to their single mode core. Due to the long length of active environments they have better heat removal of heat losses so there are not complicate cooling. These benefits have also the conventional fiber amplifiers with single mode diodes, but the main advantage of the double clad amplifiers and lasers is mainly the opportunity to use high-power multimode pumping diodes and therefore resulting lower price and high output power.

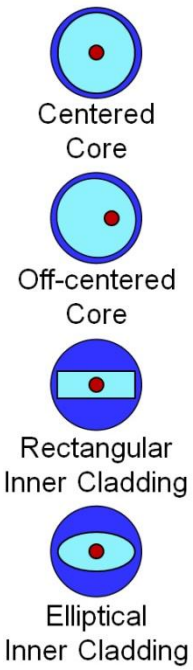

Figure 23 - Various Designs of Double Clad Fibers

The specific problem for clad pumping is to ensure effective absorption of pumping along the fiber. For example in the case of circular cross-section fiber is absorbed by pumping selectively a part, which is spreading in the center (called meridian rays), while the oblique rays (non-axial) pass the core and are not damp. Absorption of pumping is not homogeneous along the fiber, but the pumping is spreading almost without loss after absorbing meridian rays at the beginning of the fiber. Therefore, the goal is to ensure maximum absorption of pumping in the fiber, i.e. to ensure a homogeneous attenuation along the whole of fiber. This can be achieved by appropriate design of the cross section of the inner cladding that will provide the so-called chaotic dynamics of the spread of rays. In the double clad fiber with "chaotic" spreading is reaching for the statistically uniform distribution of radiation intensity on the cross. In any method of excitation after certain length of fiber there is reaching for the statistically uniform distribution of radiation intensity on the cross in the double clad fiber with "chaotic" spreading. An example of such a cross section of fiber is in [Figure 22], called D-shaped fiber. The other possible various designs of double clad fibers are show in the [Figure 23].

Another problem of the double clad lasers and amplifiers is to link up the pumping into the cladding, while maintaining the ease of conjunction the single-mode signal and the active core. Although it was described in the

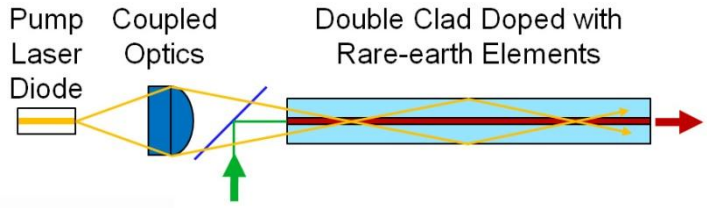

Figure 24 - Use of Volume Elements

literature several ways to solve this problem, we mention the three essential. The first is shown in the [Figure 24]; it is the use of volume elements.

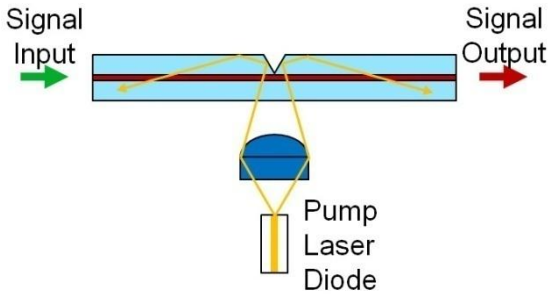

Figure 25 - V-groove

The second way is to cross-link up the pumping from the side of active fiber either by a diffraction element (such as a prism) or through the notch in the shape of V-groove [Figure 25]. The Bell Labs have developed an elegant method, using fused fiber coupler member formed from several multi-mode fibers, concentrated around one single mode fiber, called ***star coupler***, see [Figure 26]. The Institute of Photonics and Electronics developed a double clad fiber with a specific cross section, which is possible to fuse with a signal and pump fiber without any intermediate element, as described in the next chapter.

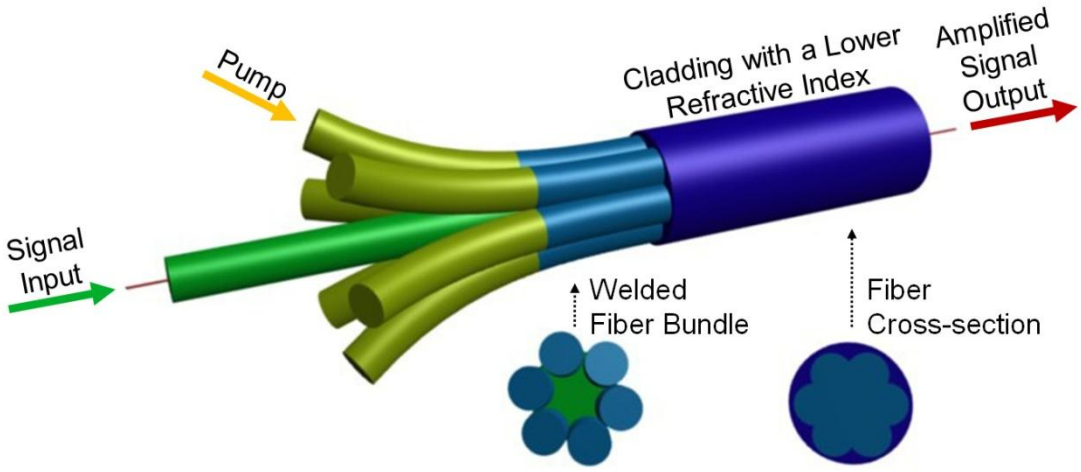

Figure 26 - Star Coupler

4.2.4 Method for end-pumping of double clad optical fiber developed at IPE

As a technique to pump is used method shown in the [Figure 27]. The advantage of such solution lies in the fact that the signal and pumping fibers are directly connected to the forehead double clad fibers with a specific shape of the cross section. The connection is realized in fiber fusion splicer. The method shown in [Figure 24] needs a special coupler. The task of coupler is to merge two signals, both pumping and signal, and with maximum coupling efficiency to the double clad fiber.

Solution, which is in [Figure 27], does not need coupler or any other intermediate element. The advantage of this solution is simpler and more affordable technology, which does not

require complicated devices for the manufacturing of couplers, or implementing of a diffractive element (V-groove) as by the method for side pumping. Another advantage of this solution is possibility of connection both pumping and signal fiber to double clad fiber with a standard fiber optic fusion splicer.

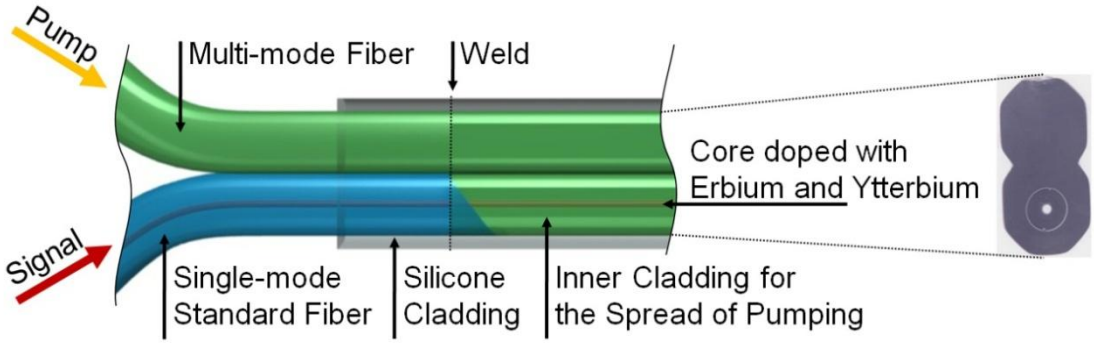

Figure 27 - Double Clad Active Fiber with Asymmetrical Cross Section

Such a possibility of connection is achieved through the cross section of the double clad fiber, which tries to copy the two fibers lying side by side. This we see in the right part of [Figure 27]. For efficient pump absorption along the fiber contributes both by asymmetrically situated core and non-circular shape. Preform of the double clad fiber is created from polished rod of the silica glass (the part designed for pump input) and polished preform with the core doped with rare-earth elements of erbium and ytterbium (the part for the signal). This preform with the core is made in IPE with technology MCVD – Modified Chemical Vapor Deposition [4.2.5.1]. The fiber pulling from preform takes place at lower temperatures than is usual for standard fibers in order to safeguard the non-circular cross section shape preform. By the pulling process, it is applied to the fiber coating of polysiloxane polymer or fluorinated acrylate. The cover must have a lower refractive index than the core of silica glass, so the inner cladding forms multimode waveguide for spreading pump light. This method has been tested with double clad fiber doped with erbium and ytterbium prepared in IPE as a fiber laser [D4] and in fiber amplifiers [D5].

4.2.5 Preform Fabrication

Although several techniques have been developed, meeting the most important conditions for fiber fabrication, such as impurity-free fiber, excellent controllability of waveguide structure, and realization of highly reliable fiber with sufficient strength, the following three methods are mainly utilized - Vapor-phase Axial Deposition (VAD), Outside Vapor Deposition (OVD), and Modified Chemical Vapor Deposition (MCVD). Our software is

developed for the analysis preform from manufacturing MCVD technique, so we just describe below only this method.

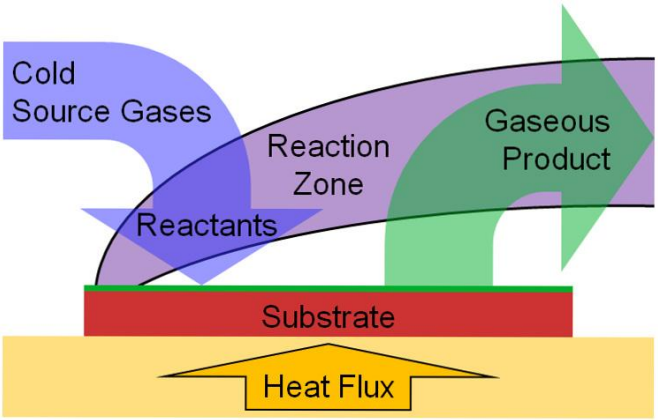

Figure 28 - Schematic illustration of CVD process

4.2.5.1 MCVD

The Modified Chemical Vapor Deposition process was developed by Bell Laboratories in 1974. The process was originally called Inside Vapor Deposition (IVD). Later, this method was significantly improved and renamed. Now is probably the major technology used for the manufacture of optical fibers. A basic principle of the method is based on chemical vapor deposition (CVD), which is a chemical process of production and deposition of material in solid state from starting materials in gaseous state through a chemical reaction used to produce high-purity, high-performance solid materials. The characteristic feature of the method is that fine glass particles are sintered immediately to transparent glass films. The principle of CVD is seen in the [Figure 28].

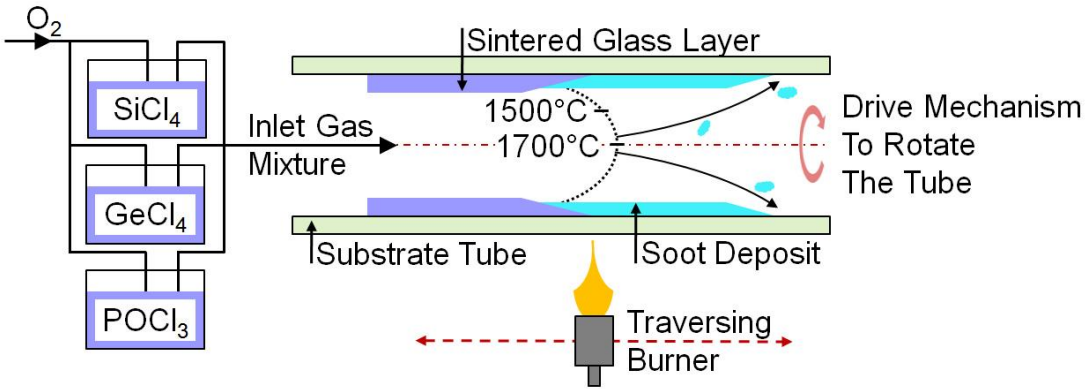

Figure 29 - Schematic Illustration of the MCVD Method

In MCVD, a mixture of $SiCl_4$, $GeCl_4$, and $POCl_3$ gases flow with a carrier gas of O_2 into a hollow silica tube about 2.5 cm diameters, which is surrounded on the outside by a heat source of the oxy-hydrogen flame. The tube is rotated with a drive mechanism. The fiery glow converts the gases into snow-like silica soot inside the tube, as shown in [Figure 29]. The sooty particles are deposited on the inner wall of the tube downstream of the flame. The particles are vitrified immediately because of the high-temperature oxy-hydrogen flame (e.g., 1500°C or more). After the layer is deposited, the burner is brought back to the starting position, and according to the needs, the mixture of reactive gases is changed. The above step is repeated and another layer is deposited.

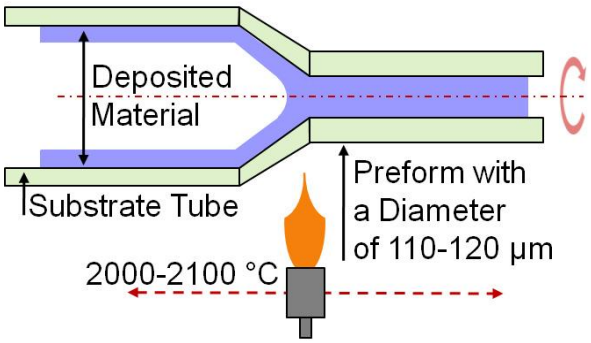

Figure 30 - Collapsing of Preform

This process is applied layer by layer to create the basic structure of optical fiber. Varying the concentration of dopants we can change the refractive index and thus create different types of fibers, such as graded-index profile. The core is formed next by changing the dopant mixture to create a vapor with a higher refractive index. After a desired quantity of glass layers is deposited, the tube is collapsed under the higher temperature condition with the same oxy-hydrogen flame into a solid rod called a preform [Figure 30]. The preform manufactured on the MCVD lathe is heated and drawn down the standard diameter of 110-120 µm. Each preform generates many kilometers of fiber. The deposited layers of SiO_2 and GeO_2 form a core. The inner cladding is formed by SiO_2 and the collapsed silica tube forms an outer cladding. All manufactured preform are tested, if they meet strict industry and internal specifications. These tests include the measurement of mechanical strength, geometric properties, and optical properties. Here are just looking to exploit our tomography software. The most important advantages of the MCVD method are that precise control of the refractive index profile is possible and a complex profile can be formed.

5 Refractive Index Profiling Methods

Knowledge of the transverse index distribution is important in both experimental preparation for research and quality control during mass production of optical fibers. On that basis, we can anticipate at least partially the most important properties of optical fibers, loss and bandwidth. Without precise methods for measuring the RIP, high quality fibers could not be made. Observed refractive index RIP is used also for selection, which preform corresponds to the proposed profile. Nonconforming preforms are excluded. We can also make some correction of the fiber properties before the process has progressed to the stage of fiber pulling. For example, the ratio of core diameter to the whole preform can be reduces by re-cladding preforms with another glass tube or increased by etching of preform part in hydrofluoric acid solution. The measured profile is used as a feedback for correction of the technological process of preparation MCVD preforms, such as the flow of carrier gas, burner flame, temperature, etc.

We can divide methods for measuring the RIP into two groups: ***interferometric methods*** and methods based on ***measuring the refractive angle of the beam***. Detailed account of these methods is given in the book of Dietrich Marcuse *Principles of Optical Fiber Measurements* [D8], from which we drew on. At the very beginning we mention *The Reflection Method*. Then we devote attention to some basic considerations of interferometric methods – without the detail equations but only highlight the principle; namely *Interferometric Slab Method* and *Transverse Interferometric Method* (TIM). In the following, we will focus on *The Refraction Angle Method* and *The Focusing Method*. At the end we mention *The Spatial-filtering Technique* used at IPE in the past.

5.1 The Reflection Method

This simple method exploits physical principle that the reflectivity of a dielectric surface depends on the difference of the refractive indices of the surrounding medium, for example, air, and the glass of the fiber. [Figure 31] shows the principle of operation.

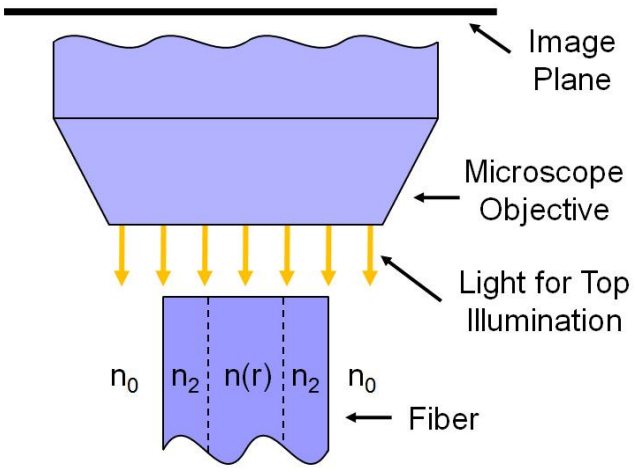

Figure 31 - Arrangement for Viewing the End Face of a Fiber

Collimated beam of light form the microscope shines at right angles on the end face of a fiber, and it is reflected upward. Differences in the reflected intensity can be observed in the image plane of the microscope. From this picture we are able to compute the refractive-index distribution.

In the simplest case, the photographic film can be used to capture the image intensities. Although in most cases, direct electrical methods for measuring light intensities are preferable, for their higher speed. Methodology for measuring the intensity is not a part of our work. Let us only mentions that monitoring the intensity of reflected light can be realized by a photodiode on the chart recorder, or an electronically scanned array of photodiodes may be used, if higher speed is required. The far end of the fiber is immersed in index-matching liquid to avoid an unwanted superposition of reflection from this end on the desired signal. Great source of error brings surface contamination with substances (e.g. grease or water), which adhering to the fiber face, because a thin film of water can distort the whole measurement.

In principle, the reflection method is applicable to fibers as well as preforms, but is inherently destructive – if the index is measured at different points along the same preform, it must be broken repeatedly. For this reason, the reflection method is useless for preform measurement; therefore we will not further deal with this method. For more information about this method we recommend to consult the book [D8].

5.2 The Interferometric Slab Method

The profiling method in this chapter is even more demanding in that it operates with very thin slab of fiber or preform. A thin slab is cut out of the fiber of thickness 0.1-0.5 mm. There are high demands on sample preparation, because the both faces of the slab must be highly parallel and flat. This disadvantage is balanced by a higher precision because methods based on interferometry are inherently very accurate; it is necessary to work with an interference microscope. In addition, there is no need for calibration; the interferometric slab method yields the difference $n(r) - n_2$, between core and cladding refractive indices unambiguously, provided the sample thickness is known and flatness and parallelism of the sample faces is assured [D8]. Although

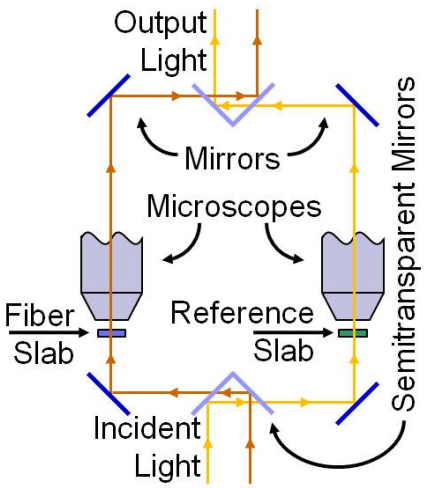

Figure 32 - Apparatus used for the Interferometric Slab Method

this method is also destructive, we see important here to mention it, because it is very accurate.

[Figure 32] shows the schema of an interference microscope. The main part consists of an interference microscope which is divided into two parallel arms so that they are perfectly matched to provide the same optical path length. The operating principle is always the same for interference measurement techniques. The incident light is divided by a beam splitter into two branches. The first beam passes through measured sample (our fiber slab) placed in one arm and the other one through the homogenous reference sample (slab) placed in the second arm of the interference microscope as shown in [Figure 32]. The different refractive indices of the two samples cause a change of the difference of optical paths, which is the basis for the interference of light output. The description of a plane wave in the publication of Dietrich Marcuse [D8] can be simplified by assuming that the propagation vector K points in z direction. We may write it in the form

Equation 5

$$E = Fe^{i(\omega t - nkz)}$$

Traveling the length of d causes a phase shift

Equation 6

$$\psi = nkd$$

If we imagine that both samples have a constant refractive index along its length, we can formulate the change in the difference of optical paths $\Delta\delta$ in the simple equation

Equation 7

$$\Delta\delta = (n_1 - n_{re})d$$

where n_1 is the index of the measured fiber, and n_{re} is the index of the reference fiber. The distance d presents the identical thickness of the slabs. It is important that the formula [Equation 5] can be used also for inhomogeneous samples, with the condition that the refractive index changes only slightly over distances comparable to the wavelength of light in the dielectric medium. We therefore generalize $n_1 = n(r)$, where $n(r)$ is the core index of the fiber at radius r. And we get relative phase shift

Equation 8

$$\Delta\psi = [n(r) - n_{re}]kd$$

where k is the free-space propagation constant and the cladding index of measured slab is equal to n_{re} – the refractive-index value of the

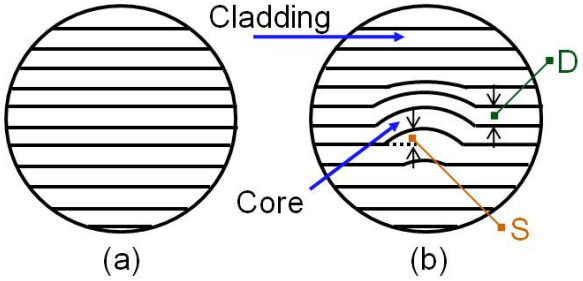

Figure 33 - Schematic Representation of Interference Fringes

reference slab. After combining the both light images by a second beam splitter we observe in the microscope the interference fringes, which indicate regions in space where the sample and reference waves are either in phase (light bands) or out of phase (dark bands). For better measurement results the two recombining wave fronts are slightly tilted relative to each other. From one dark or light band to the next corresponding band the relative phase shift of the waves is 2π. The distance D between fringes thus corresponds to a phase difference of 2π. The shift S of a fringe from its original position is associated with an additional relative phase shift $\Delta\psi$. The Schematic drawing of these interference fringes is shown in [Figure 33]. In part (a) we see straight fringes, which may indicate the absence of a preform or a preform without core. The second part (b) displays the fringe shift caused by a graded-index core. The fact that the unperturbed fringe spacing corresponds to a relative phase difference of 2π while the fringe shift S corresponds to $\Delta\psi$, may be expressed by the proportionality equation

Equation 9

$$\frac{[n(r)-n_2]kd}{S(r)} = \frac{2\pi}{D}$$

After some adjustments described in [D8], we can express the refractive-index difference between core and cladding as

Equation 10

$$n(r) - n_2 = \lambda S(r)/Dd$$

where all parameters are well known, or can be measured from the resulting image; λ expresses the vacuum wavelength. If the interference microscope is not available (e.g. due to its price – it is very expensive), it can be used the ordinary microscope with some modification of method. Although the interferometric slab method is destructive and the sample preparation is complex, it is often used to verify the accuracy of other, more convenient profiling methods, because it provides very accurate results.

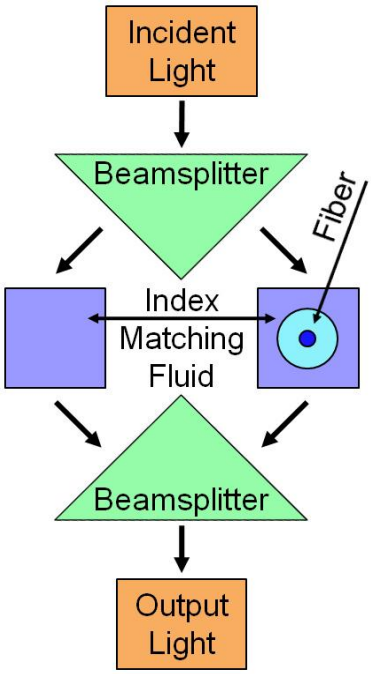

Figure 34 - Schematic representation of TIM

5.3 Transverse Interferometric Method

This method solves the problems listed in the previous chapter on the interferometric slab method. The transverse interferometric method (TIM) is nondestructive because the preform is viewed transversely to its axis under an interference microscope. This eliminates the complicated preparation of

measured samples in the form of the thin slab with flat, parallel end faces. On the other hand, the sample must be immersed in index-matching fluid. An ordinary microscope can be also used, but the following text assumes the use of interference microscope. Although the interferometric slab method has higher accuracy, TIM can better solve large refractive-index changes that are limited to small areas. Schema of TIM is very similar to the [Figure 32]. Only the preform slab is replaced by a fiber placed transversely immersed in the index-matching fluid (corresponds to the cladding), and the reference slab is replaced by identical fluid.

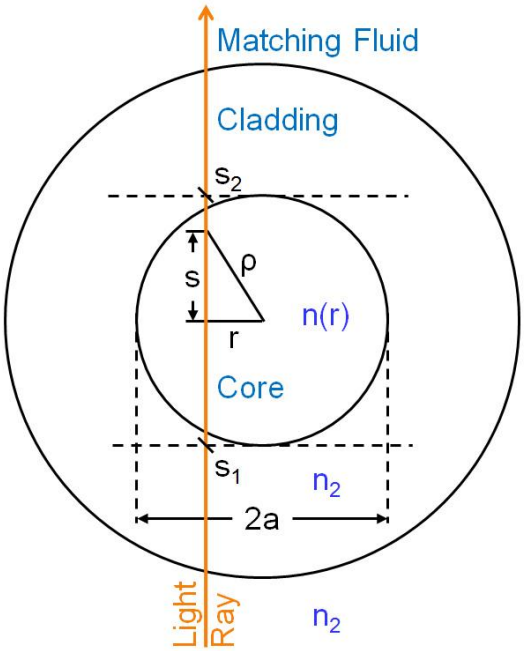

Figure 35 - Variables used in Analysis

Schematic illustration of refractive index profiling using the TIM is shown in [Figure 34]. The dark blue squares in each arm of interferometer depicted in picture shows the location of refractive index matching oil. The black arrows indicate the direction of light propagation. Green triangles represent the light splitter and coupler. The output light can be detected by CCD camera, which displays the image and store the digital image processing.

Derivation of the Relation between Refractive Index and Phase Shift

The cross-section geometry of the measured sample is shown in [Figure 35]. The refractive index along the path of the ray is no constant, so we must modify the [Equation 6], and then we can express the phase shift of the light wave along the ray as follows

Equation 11

$$\psi = k \int_{S_1}^{S_2} n(s)\, ds \rightarrow \Delta\psi = k \int_{S_1}^{S_2} [n(s) - n_2]\, ds$$

where the integration variables (S_1,S_2) represents an entrance point and an exit point of the ray. In continuation of the derivation in the same way as in the previous chapter we get a little more complicated formula

Equation 12

$$\int_{S_1}^{S_2} [n(s) - n_2]\, ds = \lambda S(r)/D$$

D and $S(r)$ have the same meaning as in the [Figure 33] – the interferogram of a preform looks very similar. The variable r indicates the distance of the fringe shift from the fiber axis.

[Equation 12] contains the unknown function $n(s) - n_2$ under the integral, which leads to the solution of integral equations. This solution is described in detail in [D8]. We mention only the final result

Equation 13

$$n(\rho) - n_2 = -\frac{\lambda}{\pi D}\int_{\rho}^{\infty} \frac{dS(r)}{dr}\frac{dr}{(r^2-\rho^2)^{1/2}}$$

where ρ is obtained from the following relationship between s, r, and ρ – see [Figure 35]

Equation 14

$$\rho = (s^2 + r^2)^{1/2}$$

The disadvantage is that TIM works on the assumption that the preform is rotationally symmetric around its axis.

5.4 The Refraction Angle Method

The preform is immersed in index-matching fluid (oil), which has the same refractive-index as the cladding. This way will simplify the whole solution, because we can only focus on the very core.

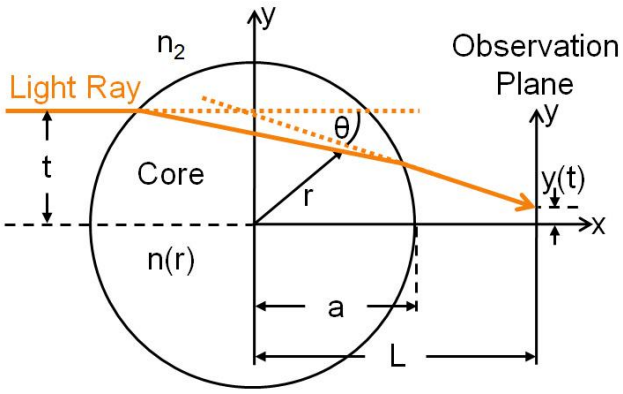

Figure 36 - Basic Setup of the Ray Tracing Method

The calculation is based on the fact that deflections of the ray are small for weak refractive-index gradients and short path lengths. All variables and the ray path are depicted in the [Figure 36]. Because of the weak refractive-index gradients and the short path lengths the ray angles can never become large, permitting us to use the simple paraxial ray equation described in the second chapter of Marcuse's book [D8]

Equation 15

$$\frac{d^2y}{dx^2} = \frac{1}{n_2}\frac{\partial n}{\partial y}$$

where $y(x)$ is the ray path. This is often referred to as the *paraxial approximation*. We consider horizontal rays that enter the fiber at an offset t as seen in the picture. To calculate the tangent of the ray angle θ at the exit point, we get

Equation 16

$$\tan\theta = \left(\frac{dy}{dx}\right)_{x=x_2}$$

Therefore, we may integrate [Equation 15] over the core to obtain

Equation 17

$$\tan\theta = \frac{1}{n_2}\int_{x_1}^{x_2}\frac{\partial n}{\partial y}dx$$

where x_1 and x_2 are the x-coordinates of the points where the light ray enters and exits the core. Angle alpha is known as deflection angle. Now we have a function of x, but the refractive-index distribution is a function of r, so we must transform the integral to an integral over r. The Substitution is suggested by the relation between r, x, and y

Equation 18

$$r = (x^2 + y^2)^{1/2} \rightarrow \frac{\partial n}{\partial y} = \frac{y}{r}\frac{\partial n}{\partial r}$$

By observation, we find that y is approximately constant during its transit of the preform, so we may do a second approximation using $y = t$ and $x = (r^2 - t^2)^{1/2}$ and get

Equation 19

$$\tan\theta = \frac{2t}{n_2}\int_t^a \frac{\partial n}{\partial r}\frac{dr}{(r^2 - t^2)^{1/2}}$$

If an observation screen is placed a distance L from the core center and $y(t) \approx y(L)$ is the measured deflection of the ray at the observation screen as a function of the input displacement, then

Equation 20

$$y(t) = t + L\tan\theta$$

Under the paraxial assumptions used above (θ is small), we can use [Equation 20] and rewrite [Equation 19] as an Abel integral equation

Equation 21

$$\int_t^\infty \frac{dn}{dr}[n(r) - n_2]\frac{dr}{(r^2 - t^2)^{1/2}} = \frac{n_2}{2Lt}[y(t) - t]$$

We can extend the integral to $\langle t, \infty)$ since $n(r) - n_2$ for all $r \geq a$. Abel integral equations such as [Equation 21] have a well-known solution, so we may write

Equation 22

$$n(r) - n_2 = -\frac{n_2}{\pi L}\int_r^\infty \frac{y(t) - t}{(t^2 - r^2)^{1/2}}dt$$

5.5 The Focusing Method

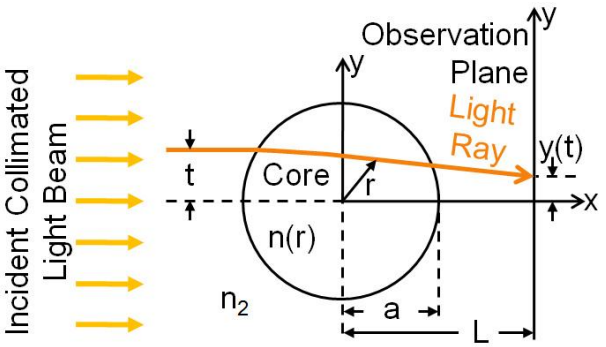

Figure 37 - The Principle of Focusing Method.

This common method is applicable equally well to preforms and fibers, and is an extension of refraction angle method, which is not very practical for use (sufficiently narrow beam, its exact location). The main difference is that the focusing method uses the lens action of the fiber or preform core. The trajectory of the input beam is strongly dependent on the focusing effect. For example GI fiber with a parabolic profile in the [Figure 7.b] acts as an ideal cylindrical lens which refracts the launching rays.

The transparent inhomogeneous object is immersed in index matching fluid and is illuminated by a relatively broad, collimated beam of incoherent, filtered light. [Figure 37] shows schematically the principle of the focusing method. The trajectory of a ray through the fiber core has been described in the previous chapter and the following derivation is based on it. The relationship between the entrance distance t of a ray (measured from the x axis) and its position $y(t)$ at the observation plan can be determined by the power distribution of the focused light.

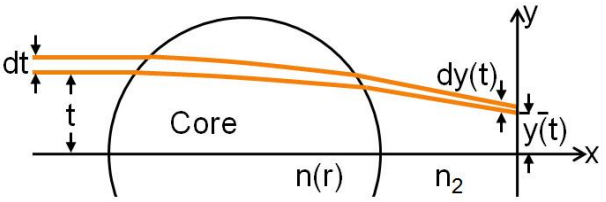

Figure 38 - Rays Focusing

The power density of the incident light has the constant value P_i, but as we see from the [Figure 38] the power density $P(y)$ at the observation screen is no longer constant. Based on the law of conservation of energy, we can write

Equation 23

$$P_i\, dt = P(y)\, dy$$

where dt is the distance between two neighboring rays prior to entering the core and dy is the spacing between the same rays at the observation plane, as indicated in the picture. And after integrating we get

Equation 24

$$t(y) = \frac{1}{P_i}\int_0^y P(y')\, dy'$$

We can integrate from zero, because when $t = 0$ is $y = 0$. Equation [Equation 22] is as follows

Equation 25

$$n(r) - n_2 = \frac{n_2}{\pi L}\int_r^a \frac{t - y(t)}{(t^2 - r^2)^{1/2}}\,dt$$

since we assume that $t - y(t) = 0$ for all $t > a$. The function $t - y$ under the integral is obtained from [Equation 24] as

Equation 26

$$t(y) - y = \int_0^y \frac{P(y')}{P_i} - 1\,dy'$$

The whole right side is transferred under the integral of the reasons for higher accuracy.

The distance L must be smaller than the focal length and larger than the radius of the core. This parameter is very important. Therefore, it is necessary to determine the exact position of the center of the preform. We can find the center of the core by moving the microscope along the direction perpendicular to the axis of the preform. When focused on the center of the core, the fringe of the preform is very clear. The distance of the image plane is obtained by backing the objective lens with a desired distance L [D9].

The precision of the focusing method is much higher than that of the Transverse Interferometric Method and is comparable to the Interferometric Slab Method. However, compared to the slab method, the focusing method is more susceptible to systematic errors which must be avoided by careful design and operation of the equipment. The calculation is dependent on the type of integration and some hints for numerical integration of [Equation 26] are listed in [D8].

5.6 The Deflection Function Measuring at IPE [D10]

To obtain the deflection angles of a laser beam that scans through a fiber preform is used at IPE the Photon Kinetics' 2600 Preform Analyzer; see [Figure 39]. The analyzer is located in the Laboratory of Optical Fibers in Prague-Suchdol. The device is connected to a PC with an interface for control and data collection.

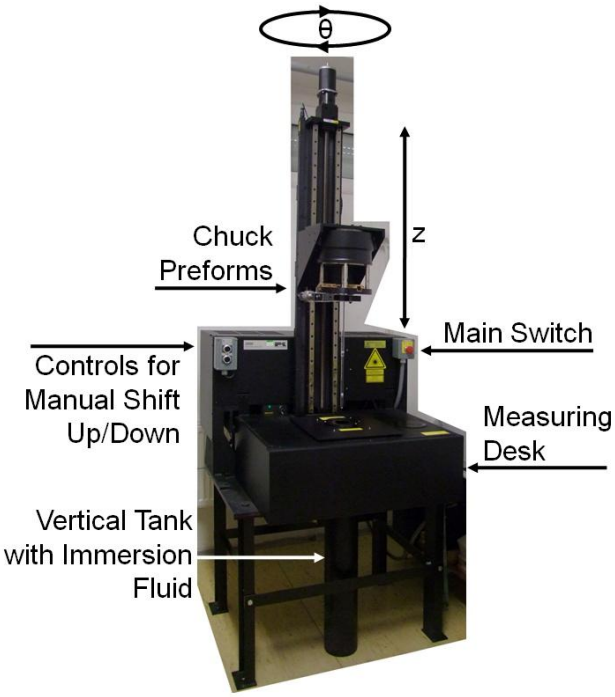

Figure 39 - PK A2600

The Analyzer Consists of Several Parts:

- preform tower with a long rail table and a preform gripping mechanism
- measuring table
- tank of index-matching oil
- Laser part - He-Ne laser at a wavelength $\lambda = 633\text{nm}$.

The tower has a precise stepper motors for automatic scrolling preforms and in the top part has a chuck for gripping of preform. This chuck can be rotated around its vertical axis with high precision of one degree of an angular rotation. Another degree of freedom is given with possibility of movement in the vertical direction (axis z). With this mechanism it is possible to measure the refractive index along the whole preform during one measurement. It is important in determining the longitudinal homogeneity of the refractive index profile.

Preform gripped in the chuck is embedded in the index-matching oil, which is in the tank. This tank is a part of measuring table, where the measurement system for deflection functions is located. The preform analyzer consists a very few controls: emergency stop switch, laser switch and the up/down buttons for manually setting the optimum height above the measuring table. Other controls are carried out by the program from PC.

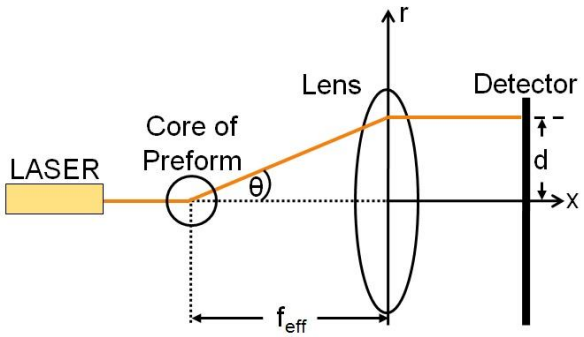

Figure 40 - Schema for Measuring the Deflection Angle at PK A2600

Measuring the Deflection Angle

Principle of measuring the deflection function shows the [Figure 40]. Laser beam is refracted by passing through the preform, is straightened using the lens, and falls on the detector at a distance d from the beginning of coordinates. Whole measuring system (laser, lens, and detector) moves together with the preform along the r-axis. The exact value of deflection angle is given as

Equation 27

$$\phi = artan(d/f_{eff})$$

Assuming that the measuring angle is very small, we can replace $artan$ with high accuracy with $asin$

Equation 28

$$\phi \cong asin(d/f_{eff})$$

where d is the displacement of the deflected laser beam from the position-sensing detector center and f_{eff} is the effective focal length of the 3-inchdiameter lens (7.62 cm). The deflection angle measurement circuitry allows the measurement of voltages V_a and V_b. These voltages are then digitized, and the value $(V_b - V_a)/(V_b + V_a)$ is computed. In terms of the displacement d of the incident beam from center, this quantity is specified as:

Equation 29

$$\frac{(V_b - V_a)}{(V_b + V_a)} = const \cdot d$$

where $const$ is a proportionality factor which can be determined by executing the calibration of the detector. Therefore, the deflection angle θ is:

Equation 30

$$\phi = asin\left[\frac{1}{const \cdot f_{eff}}\frac{(V_b - V_a)}{(V_b + V_a)}\right]$$

The effective focal length f_{eff} is a design parameter of the angle-measurement lens. The output of the measurement process is deflection function $\phi(r)$ for a certain vertical location of preform z and its turning θ. The preform analyzer PK A2600 allows to measure deflection functions automatically in succession for different longitudinal planes and angles, so the output is a set of deflection function $\phi(r, \theta, z)$.

5.6.1 Data storage

The analyzer PK A2600 is designed for industrial use, where typical measurement consists of three projections. So a small number of projections are unsatisfactory for our computer tomography. Therefore, we have modified the relevant control macros so that it can measure more projection. The measured data are stored in binary file with extension *.sav and translated using sav2txt program (Copyright Photon Kinetics, 2004) to series of text files:

BASE_system.txt - contains the global system parameters

BASE_info_xxxxx.txt - parameters for measurement xxxxx

BASE_raw_xxxxx.txt - the raw data

BASE_pwr_xxxxx.txt - the power data

BASE_def_xxxxx.txt - the deflection function

BASE_ind_xxxxx.txt - the index profile

where BASE is replaced by BASEfilename in the invocation of sav2txt and xxxxx is the measurement number.

6 Tomographic Reconstruction of the RIP using Measured Deflection Function

In the previous chapter, we analyzed the main approaches for measuring the refractive index profile of the preform. In this section we would like to continue to focus on the theory of calculation of deflection function. We will draw on the work of [D11], [D12] and [D13], where the derivation of calculation the refractive index profile is described in detail.

The deflection function gives us the dependence of the relative deviation from the angle θ, which is a direction of input laser beam into preforms as shown in [Figure 41]. Another variable ρ determines the point of entry into preform, which is the distance from the parallel line passing through the center. As we mentioned in the chapter about methods [5], the preform is immersed in immersion liquid ($n \approx 1.46$). The reason is to improve the conditions of measurement, because the cladding of preforms is composed of quartz glass, whose refractive index is approximately equal to 1.47 at wavelength of the probe beam of the HeNe laser. This will get rid of steep step changes in refractive index at the edges of preforms. Moreover, the authors [D11] derived the relation under an assumption of small differences in refractive index Δn.

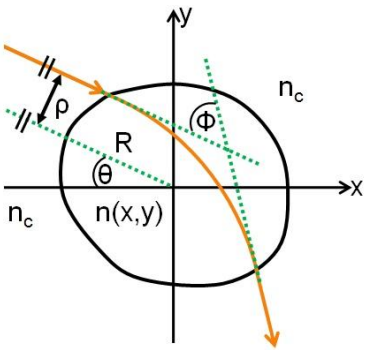

Figure 41 - Trajectory Deflection Function

If we looked at only slightly asymmetrical preforms with generally circular cross-section, we could use the widespread equation derived in work [D11]. We will mention it for its clearness and better understanding of the derivation – the index profile $f(r,\psi) = n(r,\psi) - n_c$ in polar coordinates is given according to [D11] by

Equation 31

$$f(r,\psi) = \frac{1}{2\pi^2} \int_{-\pi/2}^{\pi/2} \int_{-\infty}^{\infty} \frac{\partial \Psi(\rho,\theta)}{\partial \rho} \frac{1}{r\sin(\psi-\theta)-\rho} d\rho d\theta$$

where Ψ is the PLD-function (Path Length Difference). In the case of small difference between the maximum and minimum value of the refractive index ($\Delta n_{\max} \approx 0.04$) the beam path is approaching a straight line and we can express the PLD as deflection function [Equation 32] as we read at work [D12].

Equation 32

$$\Psi(\rho,\theta) = n_c \int_0^{\rho} \phi(\xi,\theta)d\xi + \frac{n_c\rho}{12}\phi^3(\rho,\theta) + \Delta E + \Delta G$$

where

Equation 33

$$\Delta E = \frac{\partial}{\partial\theta}\int_0^{\rho} n_c\phi(\xi,\theta)d\xi \cdot \Delta\theta$$

is a modification term. In the circularly symmetric case $\Delta E = 0$ and

Equation 34

$$\Delta G = 2\int_0^{R} n_c\phi(\xi,\theta)d\xi \cdot \Delta\theta$$

is a constatnt. The second term is negligible compared to the first ($\phi \gg \phi^3$), for a small beam deviation ϕ after passing through the preforms. We substitute [Equation 32] into [Equation 31] and partial derives by ρ and we get the following simplified expression

Equation 35

$$f(r,\psi) = \frac{n_c}{2\pi^2}\int_{-\pi/2}^{\pi/2}\int_{-\infty}^{\infty}\frac{\phi(\rho,\theta)}{r\sin(\psi-\theta)-\rho}d\rho d\theta$$

If we substitute $z = r\sin(\psi-\theta)$ in the denominator, the integral with respect to ρ may be expressed as the convolution

Equation 36

$$\frac{1}{\pi}\int_{-\infty}^{\infty}\frac{\phi(\rho,\theta)}{r\sin(\psi-\theta)-\rho}d\rho \equiv \frac{1}{\pi}\int_{-\infty}^{\infty}\phi(\rho,\theta)\cdot\frac{1}{z-\rho}d\rho = \phi(\rho,\theta) * \frac{1}{\pi\rho} = g(z,\theta)$$

where $g(z,\theta)$ is called as g-function in the following. Now we use properties of *Convolution Theorem* and *Hilbert Transform*

Equation 37

$$\mathcal{F}\{g(z,\theta)\} = \mathcal{F}\left\{\phi(\rho,\theta) * \frac{1}{\pi\rho}\right\} = \mathcal{F}\{\phi(\rho,\theta)\}\cdot\mathcal{F}\left\{\frac{1}{\pi\rho}\right\}$$

Equation 38

$$g(z,\theta) = \mathcal{F}^{-}\left\{\mathcal{F}\{\phi(\rho,\theta)\}\cdot\mathcal{F}\left\{\frac{1}{\pi\rho}\right\}\right\}$$

where $\mathcal{F}\left\{\frac{1}{\rho}\right\} = -i\pi\cdot sign(\Omega)$, $\mathcal{F}$ is *Fourier Transform*, and $\mathcal{F}^{-}$ is *Inverse Fourier Transform*. Now we just find a Fourier image of the function $\phi(\rho,\theta)$ for each projection θ and multiply it by Fourier image of the function $1/\pi\rho$. After using the inverse transform we get the g-function, which we insert into the [Equation 35], and we finally get the RIP:

Equation 39

$$\frac{n(r,\psi)-n_c}{n_c}=\frac{1}{2\pi}\int_{-\pi/2}^{\pi/2} g(r\sin(\psi-\theta),\theta)d\theta$$

In the publication *Nondestructive Measurement for Arbitrary RIP Distribution of Optical Fiber Preforms* [D12] the reconstruction algorithm is derived with [Equation 40], which is used also in our work. This formula enables accurate calculation of the substantially rotationally asymmetrical preforms.

Equation 40

$$n(r,\psi)-n_c=\int_0^{\pi} g(\rho,\theta)d\theta$$

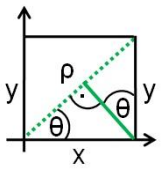

Figure 42 - Expression of ρ

where $\rho = x\cos\theta + y\sin\theta$ as shown in [Figure 42].

In contrast with [Equation 38], here is the g-function obtained directly from the PLD function:

Equation 41

$$g(\rho,\theta)=\mathcal{F}^{-}\{|k|\mathcal{F}\{\Psi(\rho,\theta)\}\}$$

A Fourier image of PLD function is multiplied by a function $|k|$, which is called spatial frequency (integration variable of Fourier transform). After expression of 2-D Fourier transformation we get

Equation 42

$$g(\rho,\theta)=\int_{-\infty}^{+\infty}\left[\int_{-\infty}^{+\infty}\Psi(\rho,\theta)e^{-j2\pi k\rho}\,d\rho\right]|k|e^{j2\pi k\rho}dk$$

For a more detailed understanding we recommend mentioned publication [D12].

7 Software Solution

Software solution can be divided into two distinct parts. The first part contains the partial routines called from the main program, which is described in the chapter [7.2.1]. The second part contains the main program.

7.1 Partial Routines

As we mentioned at the end of the Preface [1], our work follow up on the work of Eng. Slánička [D14]. We partially adjusted and incorporated his written scripts to our software for tomographic visualization in MATLAB. All the partial routines and the whole program are owned IPE and without it permission cannot be distribute, modify and use. If you are interested in them please contact the supervisor of my work.

7.1.1 The load and display functions

First we will deal with basic functions, to retrieve and display data and then we look for data editing routines in more detail.

7.1.1.1 READF.M

Syntax: `[Y] = READF()`

Description: The script opens the dialog box for selecting the files list and reads the data, returning the data in `Y` as a matrix with a corresponding number of data columns with deflection functions. There are no input arguments.

7.1.1.2 MYMESH.M

Syntax: `[ ] = MYMESH(M,AX,AY,ED)`

Description: It plots the colored parametric mesh defined by four arguments. The view point is not specified by `VIEW` and is default. The axis labels are determined by the current setting of `AXIS` with a step size of PK A2600 (standard is 5 microns) and with the integer `AX` and `AY`. The matrix `M` determines the data to display in graph. The matrix `ED` is not necessary and carries information about the edges. These edges are display like crosses in image. `ED` is a product of `LOCEDGE2()` function. This function is used for display in polar coordinates. There is no output variable.

7.1.1.3 MYMESH2D.M

Syntax: `[] = MYMESH2D(M,ISP2C)`

Description: It works similar to MYMESH with the difference that it displays the `M` matrix in Cartesian coordinates. The second input argument `ISP2C` determines if the matrix `M` has been transferred to the Cartesian, if not the `MYMESH2D` will transfer it by our `P2C` function. There is no output variable.

7.1.1.4 MYMESHC.M

Syntax: `[Y] = MYMESHC(M)`

Description: This routine prepares the data for set the axis labels in 3D. `M` is a displayed matrix. We use to see in 3D MATLAB the standard function `MESH`, which is a good tool.

7.1.1.5 MYPLOT.M

Syntax: `[] = MYPLOT(M,VAR,NAS)`

Description: Plots the line defined by vector `VAR` versus vector `M`. The argument `NAS` is used for determine the axis labels in graph. We use the graph drawing tool in MATLAB – the `PLOT` function. There is no output variable.

7.1.1.6 P2C.M

Syntax: `[Y] = P2C(M,S)`

Description: Transforms the polar coordinate data stored in polar matrix `M` (rows are the values of the radius and columns are the values of the angle) to two-dimensional Cartesian coordinate. The `Y` is a matrix x, y with the resolution 400x400.

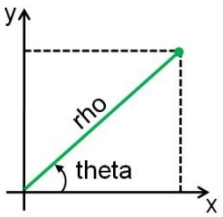

Figure 43 - Polar to Cartesian Mapping

Equation 43

$$theta = \text{atan}(x, y)$$

$$rho = sqrt(x\text{^}2 + y\text{^}2\ )$$

where ATAN and SQRT are MATLAB function.

7.1.2 Editing and Calculation Routines

Eng. Jiří Slánička wrote the kernel of routines for computer tomography, but they had to be rewritten. They were useless for automated processing in form in which we got them. We modified them and created an interface for using them in our program. For a better understanding of kernel of each script, we recommend reading the work of Eng. Slánička. Here is just a mention about the usage.

7.1.2.1 LOCEDGE2.M

Syntax: `[Y] = LOCEDGE2(M)`

Description: Reads the deflection function matrix `M` and finds in each column edges of preform. The output is a matrix `Y` which contains 3 columns - the left and right edges, and the middle.

7.1.2.2 SHIFTR1.M

Syntax: `[Y] = SHIFTR1(M,ED)`

Description: The generation of a reduced set of data `Y`. The matrix `M` contains a set of deflection function and `ED` is the output from the function `LOCEDGE2`. The routine `SHIFTR1` takes the information about edges and accordingly moves the entire data set `M` into the center. It also cuts down unnecessary data at the edges.

7.1.2.3 PLD_FCE.M

Syntax: `[Y] = PLD_FCE(M)`

Description: The script calculates the Path Length Difference of each column of deflection matrix `M`. The calculation is based on the [Equation 32], from which we derive the relationship

Equation 44

$$\Psi(\rho,\theta) = n_c A(\rho,\theta) + \frac{n_c \rho}{12}\phi^3(\rho,\theta) + n_c\big(A(\rho,\theta) - A(\rho,\theta+1)\big)$$

where $A(\rho,\theta) = \int_0^{\rho} \phi(\xi,\theta)d\xi \approx \Delta\rho \sum_{i=0}^{\rho} \phi(i,\theta)$ and the constant ΔG is neglected.

7.1.2.4 G_FCE2.M

Syntax: `[Y] = G_FCE2(A)`

Description: Calculation of the g-function from each column of PLD matrix *A*. Based on the theoretical model we use for calculating [Equation 41], where we employ the `FFT` MATLAB function. `FFT(X)` is the discrete Fourier transform (DFT) of vector `X`.

7.1.2.5 INTERP.M

Syntax: `[Y] = INTERP(O)`

Description: Data interpolation of the matrix `O` to multiple columns. The extension is set by default to 2 times, and can be set up to 50 in our program. But it significantly lengthens out the calculation - as well as a few hours.

7.1.2.6 COMPG.M

Syntax: `[Y] = COMPG(M)`

Description: It counts from the g-function the final refractive index profile. The calculation is based on the [Equation 40]. The matrix `Y` consists of the index profile in polar coordinates.

7.2 GUI (Graphical User Interface) in MATLAB

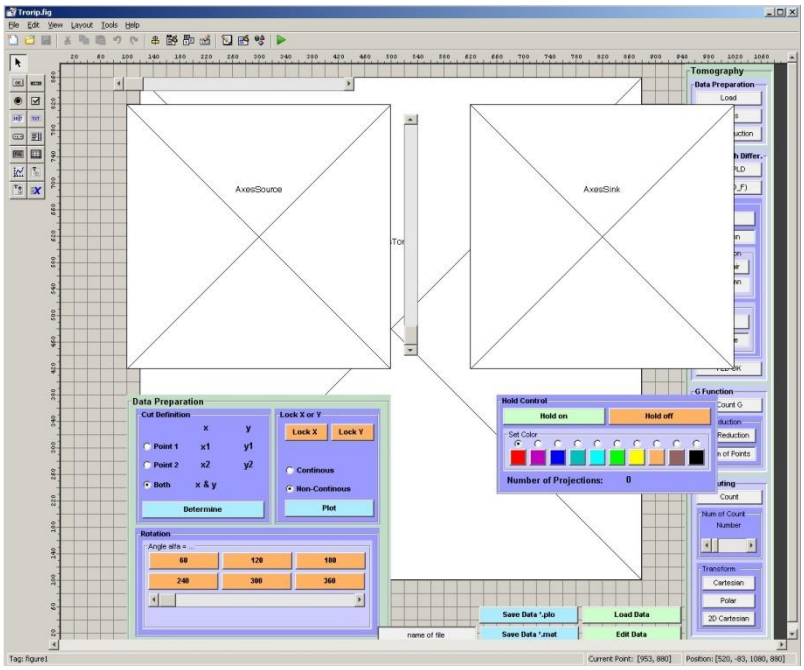

Figure 44 - GUI Design

We use a GUI in MATLAB, because it makes things simple for the end-users of the program. It is better than work from the command line interface, which can be extremely difficult and frustrating for users. The GUI Layout Editor for a graphic design project is included in MATLAB and can be opened by command `GUIDE`.

GUI is a graphical display in one or more windows containing controls, called components that enable a user to perform interactive tasks. GUI components can include menus, toolbars, push buttons, radio buttons, list boxes, axes, sliders etc. All components have the adjustable properties which can be set by Property Inspector. Our graphic design of program we can see in the [Figure 44]. We use three axis systems:

- AxesTom – to show the data editing of deflection, PLD and g functions and tomography calculation.
- AxesSource – to determine the cut of refractive index profile.
- AxesSink – to display the cut of refractive index profile.

Control buttons we grouped into three subgroups – Tomography, Data Preparation and Hold Control. The specific function of buttons we will describe in the chapter on the use of software [9].

Our GUI waits for its user to manipulate a control, and then responds to each action in turn. Each control has one or more user-written routines (executable MATLAB code) known as callbacks. The execution of each callback is triggered by a particular user action such as pressing a screen button, clicking a mouse button, selecting a menu item, or typing a numeric value. The GUI then responds to these events. The programmer provides callbacks which define what the components do to handle events.

This kind of programming is often referred to as event-driven programming. The callback execution is here asynchronous, that is, it is triggered by events external to the software. In the case of MATLAB GUIs, most events are user interactions with the GUI, but the GUI can respond to other kinds of events as well, for example, the creation of a file or connecting a device to the computer. We can code callbacks in two distinct ways, as MATLAB language functions stored in files, or as strings containing MATLAB expressions or commands. The first way is preferred, because functions have access to arguments and are more powerful and flexible.

We can build MATLAB GUIs in two ways. Use GUIDE (GUI Development Environment) or create code files that generate GUIs as functions or scripts. We prefer the first aproach for its simplicity and better picture of the general appearance. It starts with a figure that we fill with components from within a graphic layout editor. GUIDE creates an associated code file containing callbacks for the GUI and its components and saves both the figure (as a FIG-file) and the code file. The code file contains callbacks and other functions that initialize the GUI when it opens. Now we can use and write the callback in the code file.

Here is the example of our callback for the saving data:

```
% --- Executes on button press in SaveData.
function SaveData_Callback(hObject, eventdata, handles)
% hObject    handle to SaveData (see GCBO)
global Tom;
F=Tom;
nameFile = get(handles.nameOfFile,'String');

suffM = '.mat';
newF = [nameFile, suffM];
save(newF, 'F');
```

7.2.1 The Main Program – TRORIP.M

The main program consists of the initialization, many callbacks and button down functions for all components. Initialization part is changed by a GUIDE and we do not edit manually. The headers of callbacks and functions are generated automatically in the main program Trorip.m. Here is a list of callbacks, their application, and what functions are used form [7.1]:

Menu Bar:

`function New_Callback(hObject, eventdata, handles)`
- starts a new project in TR mode, see [Table 4]
- [7.1.1.1], [7.1.1.2]

`function Open_Callback(hObject, eventdata, handles)`
- opens a saved project counted in VRIP mode, see [Table 4]
- [7.1.1.2]

`function PostProc_Callback(hObject, eventdata, handles)`
- opens a saved project counted in ECD mode, see [Table 4]
- redirecting to `Load_Callback`

`function TroripHelp_Callback(hObject, eventdata, handles)`
- creates and opens dialog box describing how to use help

`function AboutTrorip_Callback(hObject, eventdata, handles)`
- creates and opens dialog box about Trorip

Tomography Reconstruction:

`function Edges_Callback(hObject, eventdata, handles)`
- prepares data for calling function to find edges
- uses: [7.1.2.1], [7.1.1.2]

`function DataReduction_Callback(hObject, eventdata, handles)`
- prepares data for calling function to reduce the data

- [7.1.2.2], [7.1.1.2]

`function PLDFunction_Callback(hObject, eventdata, handles)`
- prepares data for counting the PLD function
- [7.1.2.3], [7.1.1.2]

`function plotPLD_Callback(hObject, eventdata, handles)`
- displays PLD data in a 2D graph

`function plotPLD_s_Callback(hObject, eventdata, handles)`
- displays single column in PLD in a 2D graph

`function Repair_Callback(hObject, eventdata, handles)`
- it repairs the damaged single column in PLD

`function Cut_Callback(hObject, eventdata, handles)`
- cuts the PLD

`function PLDOK_Callback(hObject, eventdata, handles)`
- confirms the end of the work with PLD

`function GFunction_Callback(hObject, eventdata, handles)`
- prepares data for counting the g-function
- [7.1.2.4]

`function GReduction_Callback(hObject, eventdata, handles)`
- prepares data for calling function to reduce the data in g-function

`function slider1_Callback(hObject, eventdata, handles)`
- determines the number of interpolation

`function Count_Callback(hObject, eventdata, handles)`
- serves a tomography calculation
- [7.1.2.5], [7.1.2.6], [7.1.1.2]

Display Tomography Calculation:

`function Cartesian_Callback(hObject, eventdata, handles)`
- prepares data to transfer in Cartesian coordinates
- [7.1.1.4]

`function Polar_Callback(hObject, eventdata, handles)`
- prepares data to transfer in polar coordinates
- [7.1.1.2]

`function DCart_Callback(hObject, eventdata, handles)`
- to look at the data from the top in Cartesian coordinates
- [7.1.1.3]

Storage and Load Tools:

`function SaveData_Callback(hObject, eventdata, handles)`

– saves the counted data in *.mat file.

`function SaveDataPlot_Callback(hObject, eventdata, handles)`
– saves data from *Axes Sink* into the *.plo text file.

`function Load_Callback(hObject, eventdata, handles)`
– similar to `New_Callback`

– [7.1.1.1], [7.1.1.2]

`function EditData_Callback(hObject, eventdata, handles)`
– opens the ECD mode with the current counted data, see [Table 4]

– [7.1.1.3]

`function LoadData_Callback(hObject, eventdata, handles)`
– loads a saved project in ECD mode, see [Table 4]

Examination of the Calculated Data:

`function CutDef_Callback(hObject, eventdata, handles)`
– determinates the cutting plane

– [7.1.1.5]

`function sliderSourceX_Callback(hObject, eventdata, handles)`
– determines the cutting plane perpendicular to the axis X

– [7.1.1.5]

`function sliderSourceY_Callback(hObject, eventdata, handles)`
– determines the cutting plane perpendicular to the axis X

– [7.1.1.5]

`function PlotTom_s_Callback(hObject, eventdata, handles)`
– serves a menu bar

`function HoldOn_Callback(hObject, eventdata, handles)`
– enables multiple plotting in the graph

`function HoldOff_Callback(hObject, eventdata, handles)`
– disables multiple plotting in the graph

`function LockX_Callback(hObject, eventdata, handles)`
– shows the Y slider

`function LockY_Callback(hObject, eventdata, handles)`
– shows the X slider

`function rbLock1_Callback(hObject, eventdata, handles)`
– allows continual rendering when you move the slider X or Y

`function rbLock2_Callback(hObject, eventdata, handles)`
– prohibits continual rendering when you move the slider X or Y

`function PlotLockButton_Callback(hObject, eventdata, handles)`
– prepares data for plotting in the *Axes Sink*

– [7.1.1.5]

Rotation:

The following callbacks rotate clockwise the matrix on the desired angle corresponding with their name. It always takes the original matrix and rotates it.

```
function Alfa60_Callback(hObject, eventdata, handles)
function Alfa120_Callback(hObject, eventdata, handles)
function alfa180_Callback(hObject, eventdata, handles)
function Alfa240_Callback(hObject, eventdata, handles)
function Alfa300_Callback(hObject, eventdata, handles)
function alfa360_Callback(hObject, eventdata, handles)

function sliderAlfa_Callback(hObject, eventdata, handles)
```

– It rotates the matrix according to the desired angle, set on the slider.

Color:

These callbacks are assigned to radio buttons to set the color for plotting in *Axes Sink*.

```
function rb1_Callback(hObject, eventdata, handles)
function rb2_Callback(hObject, eventdata, handles)
function rb3_Callback(hObject, eventdata, handles)
function rb4_Callbak(hObject, eventdata, handles)
function rb5_Callback(hObject, eventdata, handles)
function rb6_Callback(hObject, eventdata, handles)
function rb7_Callback(hObject, eventdata, handles)
function rb8_Callback(hObject, eventdata, handles)
function rb9_Callback(hObject, eventdata, handles)
function rb10_Callback(hObject, eventdata, handles)
```

The following functions have the similar use. Besides the color they also ensure a check on the appropriate radio button.

```
function col1_Callback(hObject, eventdata, handles)
function col2_Callback(hObject, eventdata, handles)
function col3_Callback(hObject, eventdata, handles)
function col4_Callback(hObject, eventdata, handles)
function col5_Callback(hObject, eventdata, handles)
function col6_Callback(hObject, eventdata, handles)
function col7_Callback(hObject, eventdata, handles)
function col8_Callback(hObject, eventdata, handles)
function col9_Callback(hObject, eventdata, handles)
function col10_Callback(hObject, eventdata, handles)
```

Help Function

All components in GUI have their help function, which is designed as a response to pressing the right mouse button over the component. Example of such function is:

```
function nameOfFile_ButtonDownFcn(hObject, eventdata, handles)
% hObject    handle to nameOfFile (see GCBO)
helpdlg('Enter desired name.','Name of File');
```

7.3 Standalone application

In this part we describe the design and installation of standalone application without using MATLAB environment. Our knowledge we learned from the MathWorks websites, where good demos and webinars are offerd, and we also recommended this websites [W6] for better understanding. Therefore, the following text is inspired from that source with the addition of our own experience. Important notice - MATLAB Compiler is not in the basic package of MATLAB, but its optional paid tool.

7.3.1 MATLAB® Compiler™

This tool lets us share our MATLAB application as an executable or a shared library, that use a runtime engine called the MATLAB Compiler Runtime (MCR). The MCR is provided with MATLAB Compiler for distribution with your application and can be deployed royalty-free.

Key Advantages

- Lets us distribute standalone application - without running the entire suite.
- Save Money - no need to purchase a MATLAB license for each workstation, where we want to use our applications.
- Lets us use MATLAB based algorithms in other programming languages and technologies.
- Possibility distribution of MATLAB code, which cannot be viewed or modified.

MATLAB Compiler is really a great advantage for the usage of MATLAB code, because it significantly reduces application development time by eliminating the need to manually translate our code into a different language. If we want to integrate into C or C++, MATLAB Compiler provides an interface to use our code as a shared library. MATLAB builder products (available separately) let us package our MATLAB applications as software components, such as Java™ classes, .NET components, or Excel® add-ins, for use within other applications. We do not have space here to deal with this tool in more detail, so we bring only a short tutorial, how to use this tool and how to install our application on another workstation, where MATLAB is not installed.

7.3.2 Compilation

First, we recommend checking all the features of the program and debugging. We have two options for compilation - manually from the command line or by using the Deployment Tool. We suggest using the first option only if we translate one complete m-file. The second option is better, if we have more complex project with multiple m-file. The Deployment Tool is a graphical user interface (GUI), which is provided with MATLAB Compiler. The GUI opens, after entering `deploytool` at the command prompt. Then we create a new deployment project using the Deployment Project dialog, where we type the name and the location of our project, and select one of the targets – Standalone Application, Windows Standalone Application, C Shared Library, or C++ Shared Library. After we choose the second, GUI opens and saves a new project with extension *.prj.

On the Build tab we click on Add File and select the main m-file. The MATLAB Compiler has the tools to find and add all the files used in our application, but if we want to be sure we can add it manually. We can also attach pictures, data and other files. When we complete our changes, we click on the Build button on the Build tab. The compilation takes a few minutes. If the compiling process is complete (it can takes a few minutes), we find in our directory a new folder with the name of our project and two subfolders – distrib and src. Src is used to store information about compilation. The program and readme file is stored in the distrib folder.

7.3.3 Installation

Before end users can run MATLAB Compiler-generated components on their machines, they need to install the MCR. It is necessary to install it on a deployment machine only once. MCR is a standalone set of shared libraries that enable the execution of m-files. The MCR provides complete support for all features of MATLAB without the MATLAB GUI. After the installation of the MCR we set the path properly.

We add the MCR directory to the environment variable by opening a command prompt and issuing the DOS command set

```
PATH=<mcr_root>\v710\runtime\win32;%PATH%
```

where `<mcr_root>` is the directory where MCR is installed on the target machine. Alternately, for Windows, we add the following pathname

```
<mcr_root>\v710\runtime\win32
```

to the PATH environment variable, by doing the following:

1. Select the My Computer icon on our desktop.
2. Right-click the icon and select Properties from the menu.
3. Select the Advanced tab.
4. Click Environment Variables.

Files Necessary for Deployment

- Our compiled exe file.
- MCR Installer. For locations of all MCR Installers, run the `mcrinstaller` command prompt in MATLAB. (Only if the MCR is not installed on a deployment machine.)
- The text file `<name>.exe.manifest`, where `<name>` is the name of our program.
- The readme file, where we described the function and usage of our program. *(This is not necessary to run the program, but it belongs to a programming culture.)*

In version of MATLAB r2009b there is a bug with connection to runtime compiler at the workstation, where we ran a standalone application. We can resolve this error with the text file `<name>.exe.manifest`. This text file is added to the directory with the program and has the content:

```
<?xml version='1.0' encoding='UTF-8' standalone='yes'?>
<assembly xmlns='urn:schemas-microsoft-com:asm.v1'
manifestVersion='1.0'>
  <dependency>
    <dependentAssembly>
      <assemblyIdentity type='win32' name='Microsoft.VC80.CRT'
version='8.0.50727.762' processorArchitecture='x86'
publicKeyToken='1fc8b3b9a1e18e3b' />
    </dependentAssembly>
  </dependency>
</assembly>
```

For more information about the *.manifest file look at [W7].

8 Testing the Theoretical Deflection Function

This chapter is devoted to theoretical verification of our software. First we created a RIP of a preform from which we calculated the optical path length difference function. From this PLD function we computed with our MATLAB software the RIP, which was compared with the original. To verify we chose the "gradient" preform with a parabolic profile which can be written as equation

Equation 45

$$n(r) = \left(1 - \frac{r^2}{R^2}\right) n_{max} \Leftrightarrow r < R$$

$$n(r) = 0 \Leftrightarrow r \geq R$$

where n_{max} is a maximum refractive index and R is a radius. We chose $n_{max} = 0.012$ and $R = 3$ mm.

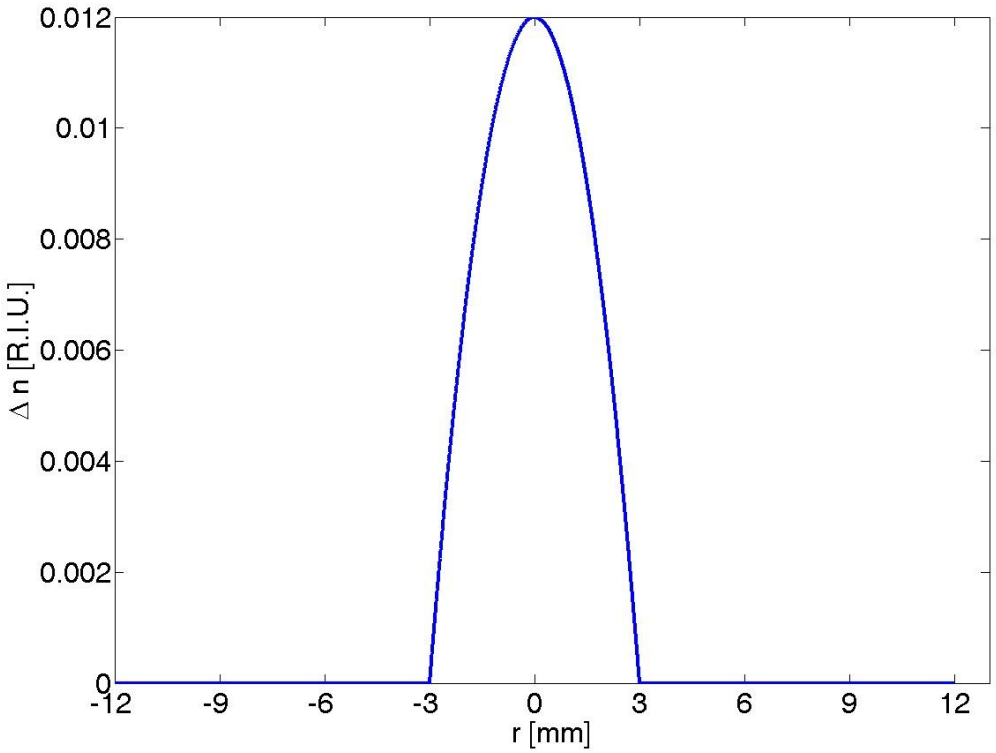

Figure 45 - The RIP of Theoretical Function

In general the optical Path Length Difference is proportional to the time required for light to travel between two points a, b:

Equation 46

$$PLD = \int_a^b n(s)ds$$

Our RIP is circularly symmetric, so we can write

Equation 47

$$PLD(r) = \int_{-b}^{b} n(r)\,dr \equiv |symmetry| \equiv 2\int_{0}^{b} n(r)\,dr$$

We substitute the formula, $b = \sqrt{R^2 - \rho^2}$ and $r = \sqrt{\rho^2 + x^2}$

Equation 48

$$PLD(\rho) = 2\int_{0}^{\sqrt{R^2-\rho^2}} n_{max}\left(1 - \frac{\rho^2 + x^2}{R^2}\right)dx = 2n_{max}\int_{0}^{\sqrt{R^2-\rho^2}} \frac{R^2 - \rho^2 - x^2}{R^2}\,dx$$

$$= \frac{2n_{max}}{R^2}\left[(R^2 - \rho^2)x - \frac{x^3}{3}\right]_0^{\sqrt{R^2-\rho^2}} = \frac{2n_{max}}{R^2}\left\{(R^2 - \rho^2)^{\frac{3}{2}} - \frac{(R^2 - \rho^2)^{\frac{3}{2}}}{3}\right\}$$

$$= \frac{4n_{max}}{3R^2}(R^2 - \rho^2)^{\frac{3}{2}}$$

We clone this function 44 times, because we count the RIP from 45 projections. In the [Figure 46] we see the calculated RIP with TRORIP in Cartesian coordinates. *(We skip in the Trorip the calculating PLD functions, because the input functions are not the deflection but directly PLD functions.)*

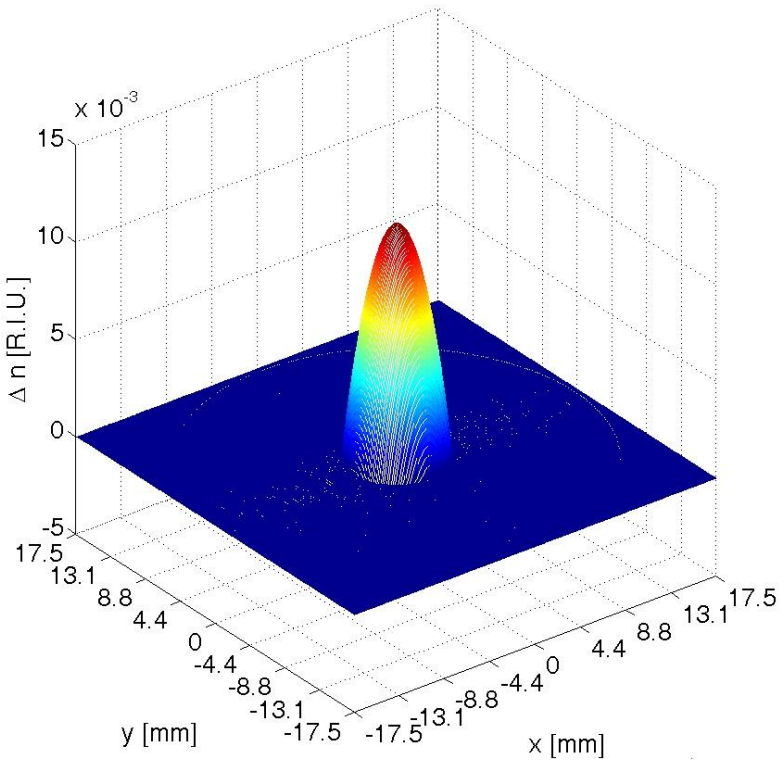

Figure 46 - The Counted RIP

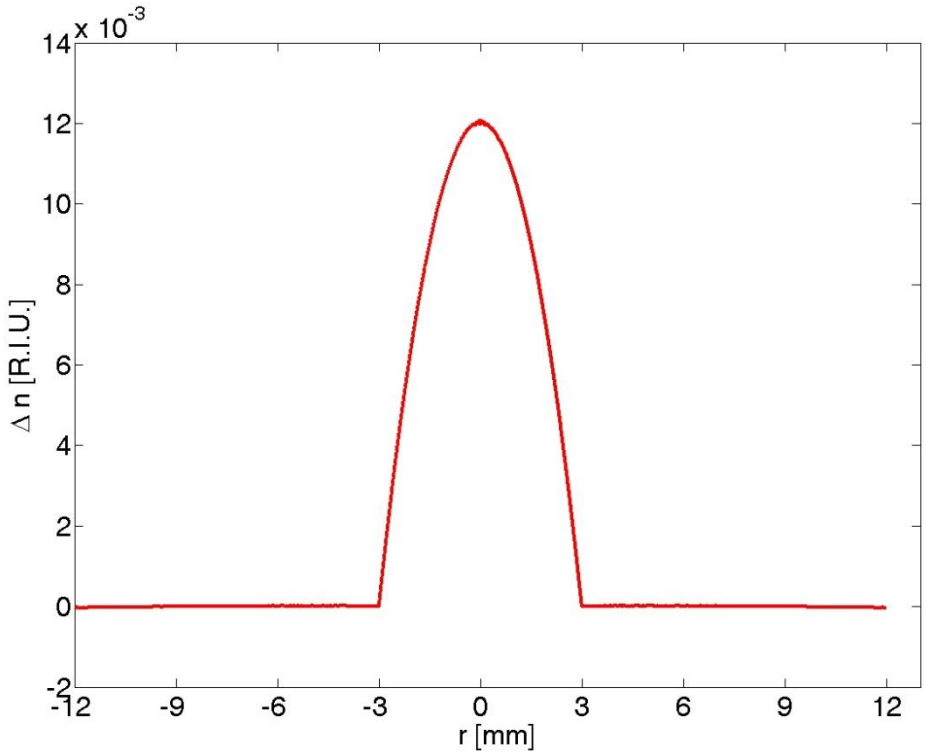

Figure 47 - Refractive Index in Perpendicular Cut form [Figure 46]

In the picture bellow we see the difference between the RIP of theoretical function from the [Figure 45] and the calculated RIP with our software.

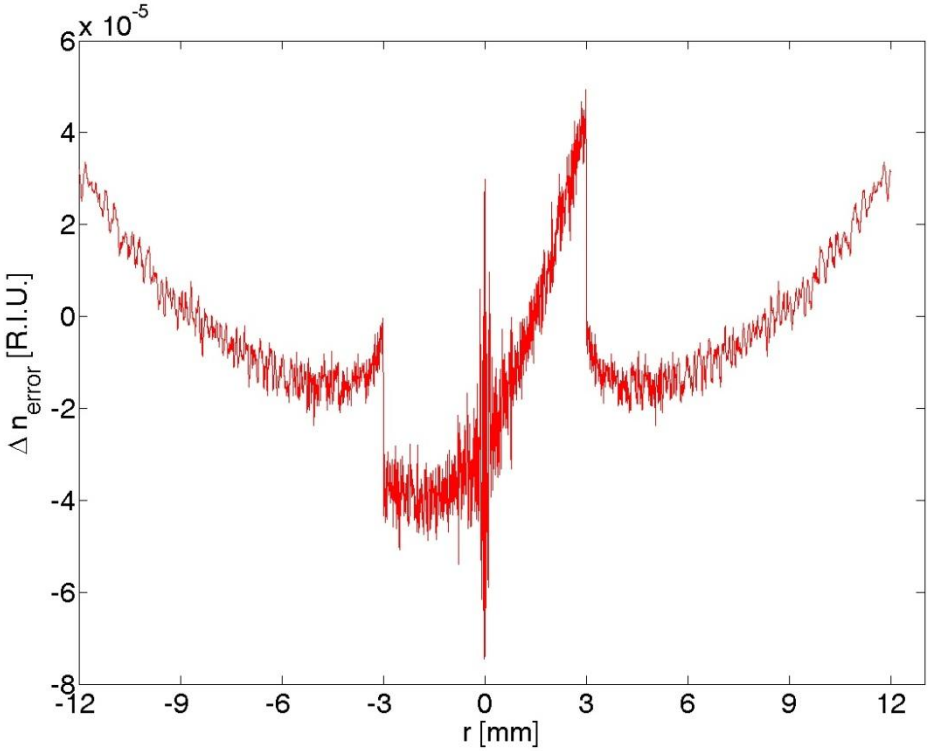

Figure 48 - The Refractive Index Difference

9 Trorip User Manual

We describe here the usage and work of the program TRORIP. Images are illustrative only, and some texts may not be readable for its small size. We assume that we have measured data of deflection functions (in the range of angles from 0 to 180) from the preform analyzer PK A2600 in the text files [5.6.1]. For example:

```
939a46_def_00000.txt
939a46_def_00001.txt
…
939a46_def_00022.txt
```

If we expect more complicated RIP, we recommend scan the multiple projections, with one or four degrees step. Symmetric preforms just scan for ten degrees.

9.1 Quick Overview

The program name TRORIP is an acronym for **T**omographic **R**econstruction **o**f **R**efractive **I**ndex **P**rofile, a notation used in my thesis title. The program is divided into two parts. One part is the *Dump Window* with error and operations. The second window is the GUI, which has three modes. The first mode is for Tomography Reconstruction (TR), the second for the Viewing the Refractive Index Profile (VRIP), and the third for the Examination of the Calculated Data (ECD). We can switch between modes using the menu controls. Menu item *File* in the Menu Bar allows just three actions:

Table 4 - Menu Bar

Option	Description	Shortcut	Mode
New	Start new calculation project.	Ctrl+N	TR
Open	Open measured data to be processed.	Ctrl+O	VRIP
PostProc	Analyze counted data.	Ctrl+P	ECD

9.1.1 Tomographic Reconstruction

When we start the TRORIP we just switch to that mode. In the [Figure 49] we see this basic operating mode, which consists of the menu bar, the figure toolbar, the panel with buttons for controlling the tomography calculation, the display area, and the storage and load tools. The panel with Computer Tomography Tools changes each step of calculating. These changes lead users intuitively how to proceed step by step.

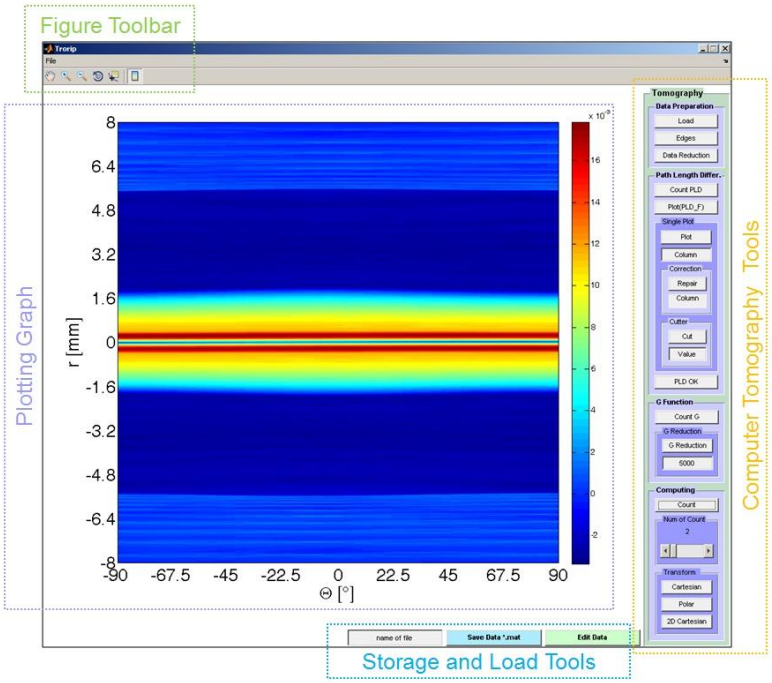

Figure 49 - Tomography Reconstruction

Figure Toolbar

These tools enable us to explore data interactively and is composed of the following icons:.

Figure 50 - The Figure Toolbar

The list below describes the different tools from left to right.

- ***Panning*** – We can move our view of a graph up and down as well as left and right with the pan tool. Panning is useful when we have zoomed in on a graph and want to translate the plot to view different portions.
- ***Enlarging the View*** – Zoom in, zoom out is useful to see greater detail in a small area.
- ***Rotate 3D*** — Interactive Rotation of 3-D Views
- ***Data Cursor*** — Data cursors enable us to read data directly from a graph by displaying the values of points we select on plotted lines and images.
- ***Colorbar*** – It adds a new vertical colorbar on the right side of the current figure and resizes the current axes to accommodate the colorbar.

Storage and Load Tools

We have here one editable text field and two button. If we want save calculation enter the file name into the text field and push "`Save Data *.mat`".

Figure 51 - Storage Tools

The second button switches the program to ECD mode and loads the counted data into it.

Plotting Graph

The Plotting Graph is a workspace where we are drawing each intermediate calculation.

Computer Tomography Tools

This panel is the main part of program. The individual keys are grouped into 4 subgroups – Data Preparation, Path Length Difference, G Function, and Computing [Figure 52]. Now, we will show the calculation and work with the program in each step.

At the beginning we will start a new calculation. We select the menu *File/New* or push `LOAD` on the panel Data Preparation. This will open a schematic in the current directory, where we find our desired set of deflection function and choose the first file: `*_def_00000.txt` [5.6.1]. Now in the *Plotting Graph* we see our deflection function, [Figure 53.a].

Measured data from the preform analyzer PK A2600 must be analyzed and usually also modified before the calculation of PLD function. We can divide the process of modifying into Edge Search (button `Edges` – [Figure 53.b]) and Correction the Shift of deflection function (button `Data Reduction` – [Figure 53.c]).

As we can note, another panel appeared below – *Path Length Difference*. The button `Count PLD` start calculating the PLD functions – the result is in the [Figure 54.a]. If we want look at the PLD function in Cartesian coordinates, use the button `Plot (PLD_F)` - [Figure 54.b]. There are no real units on the x-axis, but the number of points. A simple estimate of the cut is the main reason.

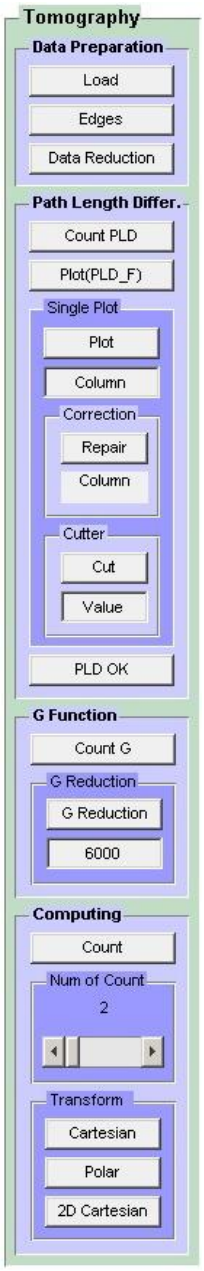

Figure 52 - Button Panel for Tomography

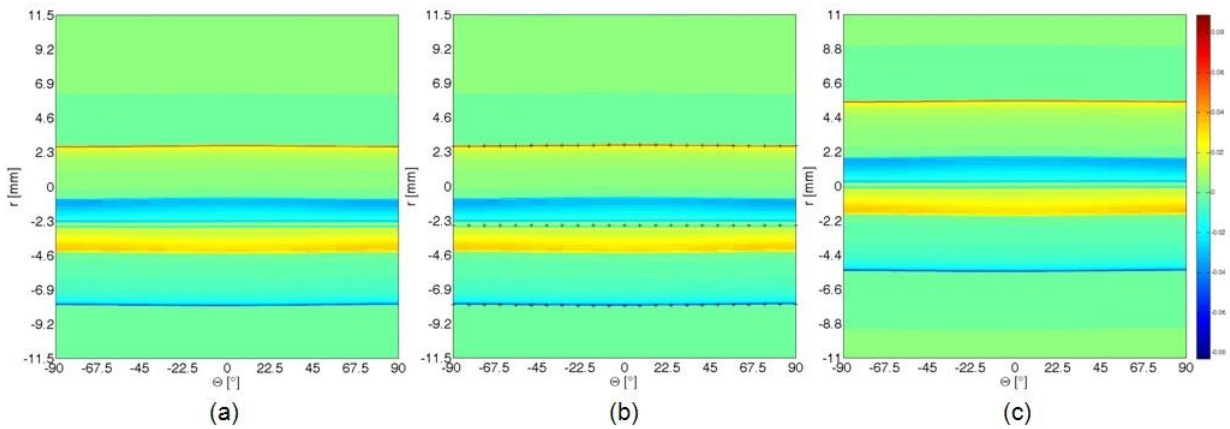

Figure 53 - Plotting Graph

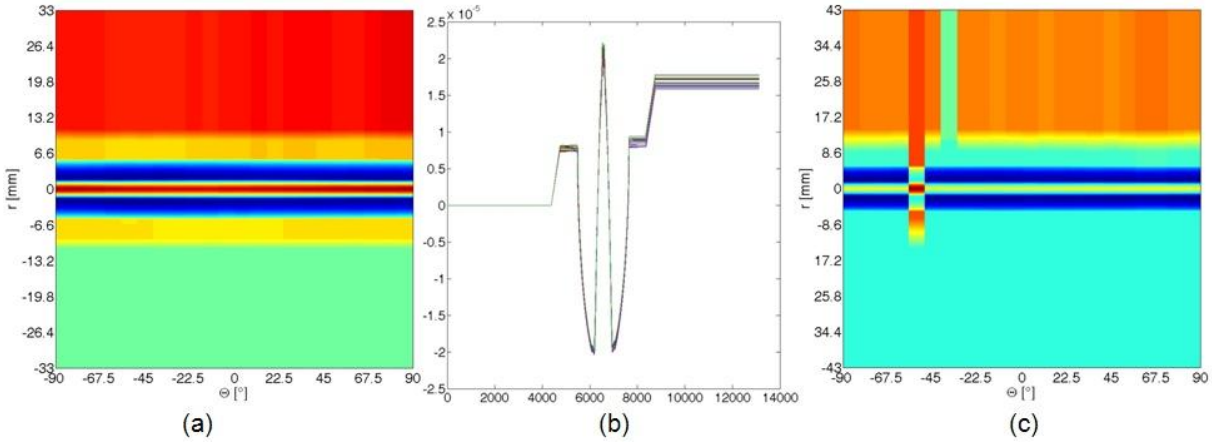

Figure 54 - PLD Function

The device PK A2600 has sometimes a problem with focusing onto the preform, therefore the output data may contain errors as we see in the [Figure 54.c], where two PLD functions are apparently wrong (in the first third of the graph). Panel *Single Plot* is used to repair these errors. First, we image with the button `Plot` a key function, which we are interested, and then correct it with button `Repair`. Function is interpolated from the surrounding proper PLD functions. If we do not need more repair the PLD, we can go to the g-function. On the panel *G Function*, press `Count G`.

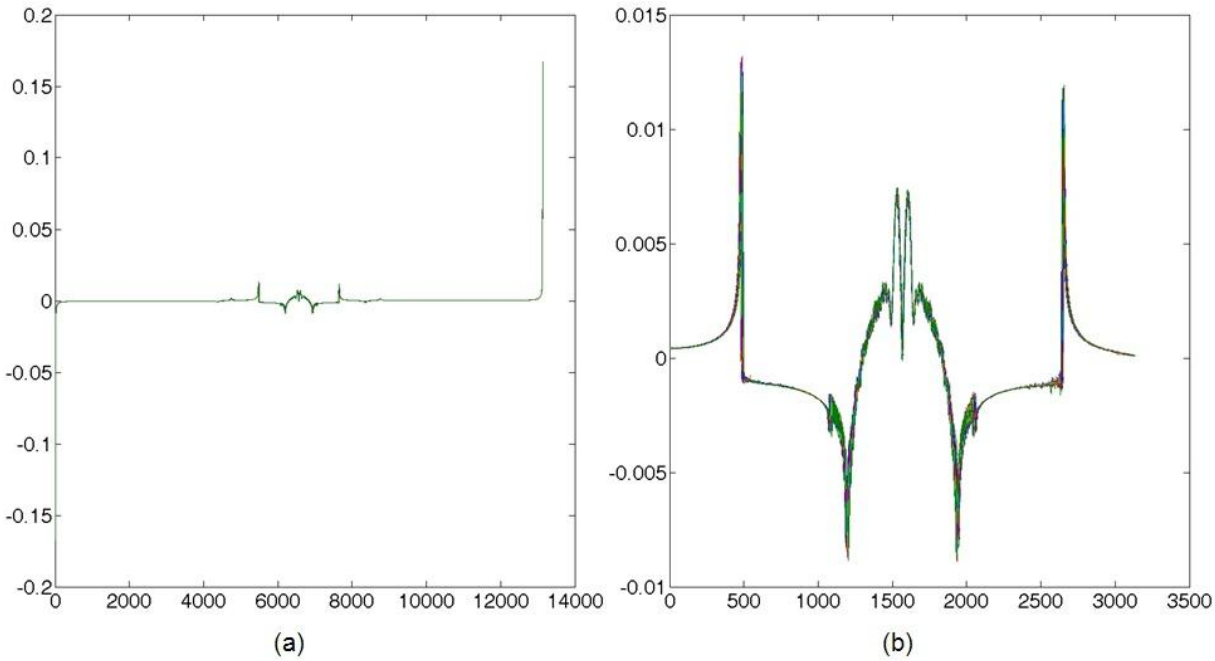

Figure 55 - G Function

We see our counted g-functions in the *Plotting Graph*. The subpanel *G Reduction* has one editable text field and one button `G Reduction`. As we see in the [Figure 55.a], most points of the function are zero; so our calculation is interesting only in the center of g-functions. We

can cut it symmetrically on both sides, when we write the required number of points and push a button; [Figure 55.b]. If we do not need more cut the g-function, we can continue. On the *Computing* panel is one pushbutton and one subpanel with a text field that depends on the slider. We set with this slider the number of interpolation between g-functions for the final calculation of the RIP. The default value is set to 2, which means that the number of g-functions we extend to double. The maximum extension is 50 times.

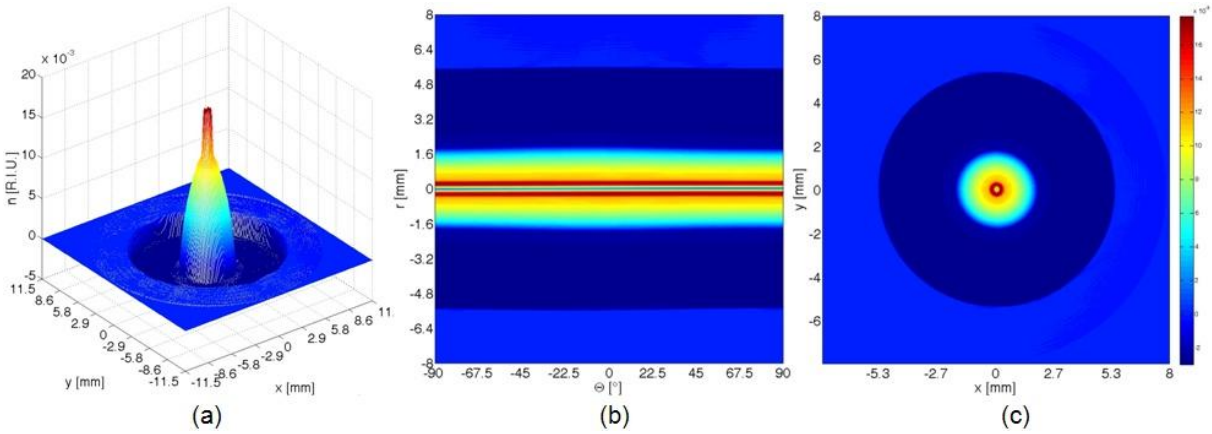

Figure 56 - Refractive Index Profile

A higher number of interpolations mean a higher requirement for computing time. The calculation starts after pressing `Count`, which can take a few minutes; with the higher number of deflection function and interpolation tens of minutes. First we recommended to calculate the RIP with default multiple of 2 and then to increase the number. In the *Dump Window* we see the execution phase. After calculating will appear the new panel *Transform* and in the *Plotting Graph* the RIP in the polar coordinates. We have on the panel three possibilities how to view the RIP – in Cartesian [Figure 56.a] and polar [Figure 56.b] coordinates and in the 2-D Cartesian, where the third axis is indicated with color (so-called contour color plot) [Figure 56.c].

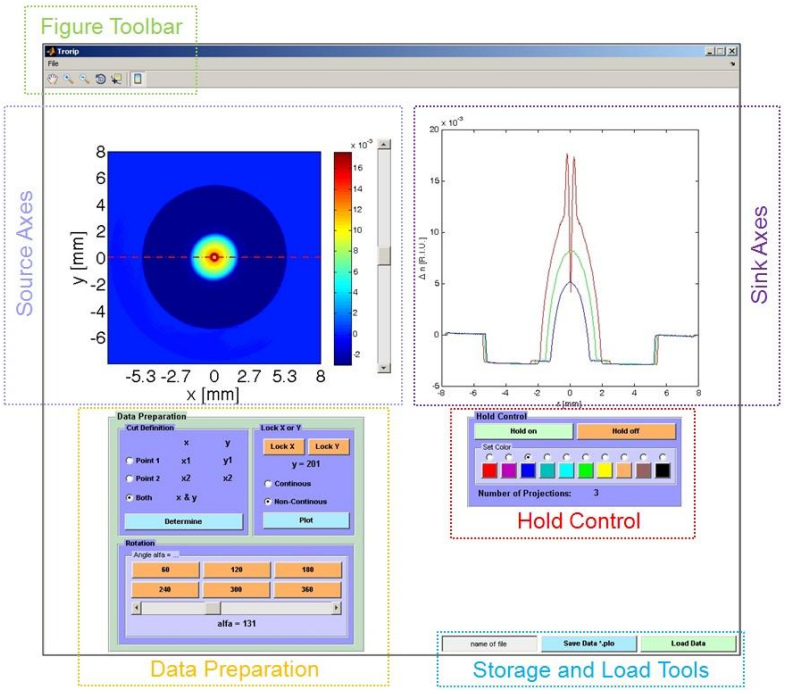

Figure 57 - Examination of the Calculated Data

If we want to save the result, we type the name into the editable text field below and press `Save Data *.mat`. The program saves the data in the MATLAB file. Now we can switch to the ECD.

9.1.2 Examination of the Calculated Data

We can turn this mode with the button `Edit Data`. If we want to load another data, we select the menu *File/PostProc*. This will open a schematic in the current directory, where we find our desired file (`nameOfFile.mat`). Now in the *Source Axes* we see the RIP like in the [Figure 56.c] – we chose this look for its simplicity in defining cut. In the [Figure 57] we see the ECD window, which consists of the menu bar, the figure toolbar, the panel with tools for preparing data, the second panel for hold control of plotting, two axes – the *Source Axes* and *Sink Axes*, and the storage and load tools.

Data Preparation

This panel has three subpanels – *Cut Definition*, *Lock X or Y*, and *Rotation*. We set with the first one the cutting plane. If we press `Determine`, the program reads the two points according to a mouse right-click on the *Axes Source*. The cut is shown in the picture like a dashed line and the data is plotting in the *Sink Axes*. We can determine first, second, or both points. Actual coordinates of the points are shown on the same subpanel in the x and y columns. If we want to make vertical or horizontal slices, we use the second panel for locking one of coordinates. We set the cut position via the slider x or y surrounding the *Source Axes*. The radio buttons `Continuous` and `Non-Continuous` assign, if the data will draw on each shift of the cutting plane in *Axes Sink*, or after pressing a `Plot`. We can also rotate the picture via the tools on the *Rotation* subpanel. Buttons define the angle of rotation according to their names, the slider for each degree 0-360°.

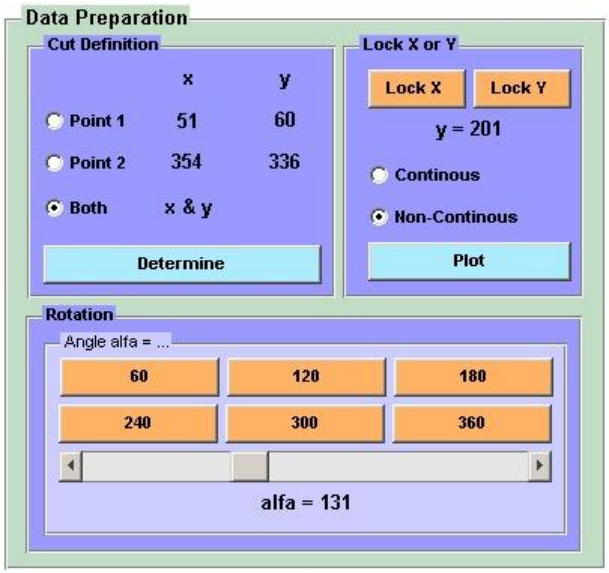

Figure 58 - Data Preparation

Hold Control

We can plot more than one projection in the *Sink Axes*. For this purpose we use the tool *Hold Control*. We can retain current graph in the figure using `Hold on`, or reset axes

properties to their defaults before drawing new plots using `Hold off`. The subpanel *Set Color* set the color property of the plotting data. And the text field `Number of projection` shows the number of line in the *Axes Sink*.

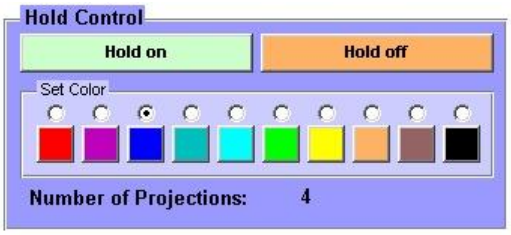

Figure 59 - Hold Control

Storage and Load Tools

If we want to save the data in the *Axes Sink*, we type the name into the editable text field below and press `Save Data *.plo`. The program saves the data in the text file accessible to other programs.

9.1.3 Viewing the Refractive Index Profile

This mode has the similar window to the TR. We can turn this mode by selecting the menu *File/Open*. This will open a schematic in the current directory, where we find our desired file (`nameOfFile.mat`). Now only the subpanel *Transform* is shown for viewing the RIP and the `Storage and Load Tools`.

9.1.4 Trorip Help

All components in Trorip have the help dialog box, which can be opened using the right mouse button. Menu item *Help* in the Menu Bar allows just only actions:

Table 5 - Menu Help

Option	Description	Shortcut
Trorip Help	Open small help dialog box of the program.	Ctrl+H
About Trorip	Open dialog box with program description.	Ctrl+A

10 Examples of preforms

Here we want to present four different types of preforms calculated by our software Trorip. All these preforms we measured for testing Trorip on the PK A2600 in Suchdol this spring.

- ***SG105*** **–** The first type is a multimode preform with the jump profile. This sample was measured in 45 projections with four degrees step.
- ***SG939*** **–** The second is gradient fiber with a single mode core. This sample was measured in 45 projections with four degrees step.
- ***SG44*** **–** This gradient preform is with highly elliptical core. It was also measured in 45 projections with four degrees step.
- ***SG827*** **–** The last sample is the most difficult to calculate. It is a composite preform of "stadium" – like cross section for cladding pumped lasers with a core doped with Yb, as described in Chapter [4.2.4]. Due to complex geometry, we chose a higher resolution and measured from 180 projections in one degree step.

10.1 Preform SG105: SI

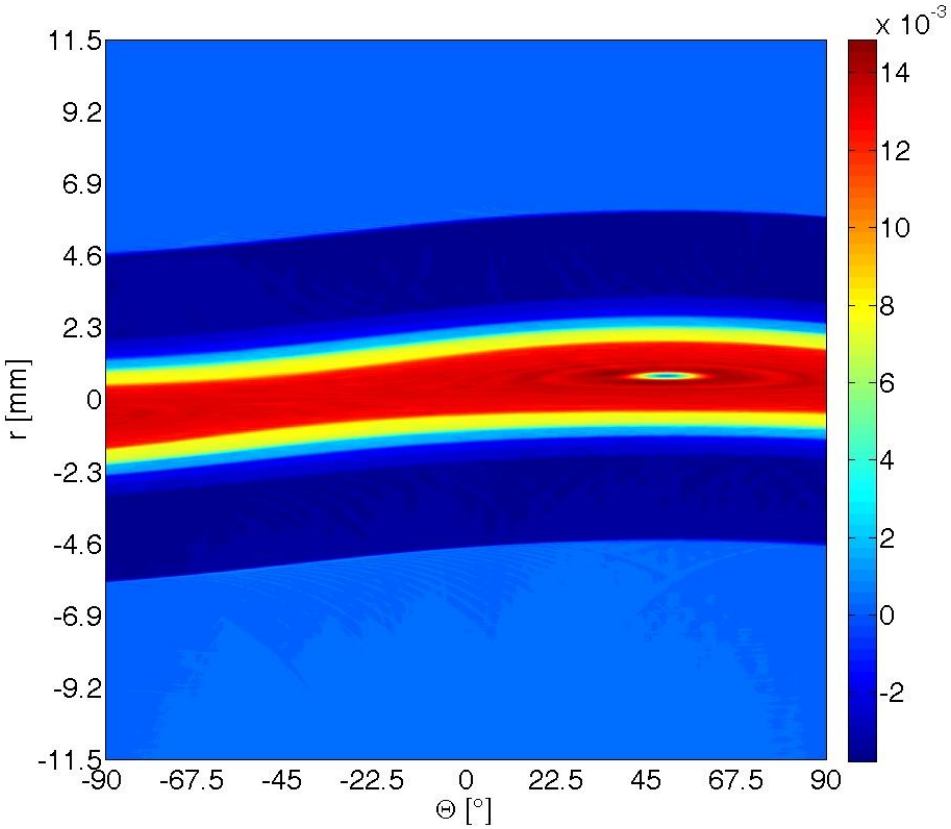

Figure 60 - SG105 in polar coordinates

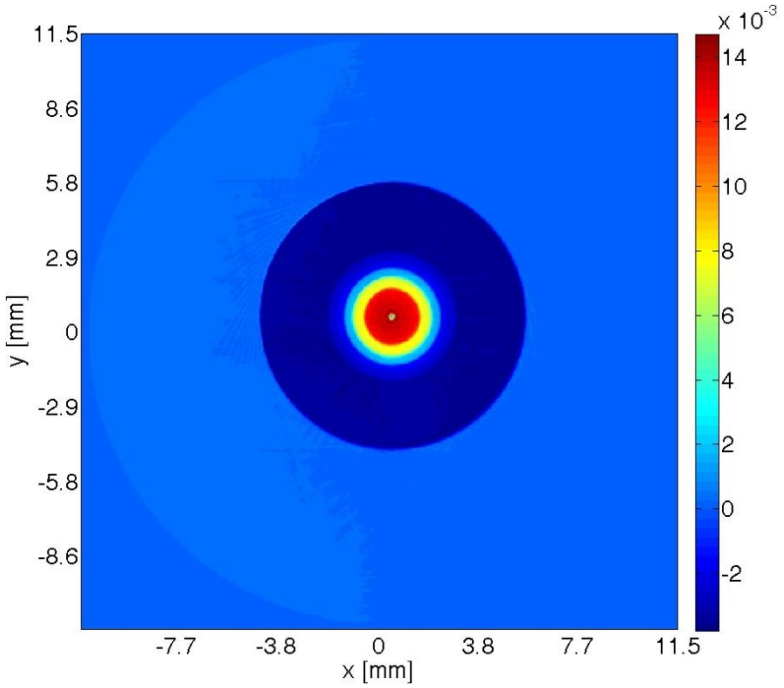

Figure 61 - SG105 Contour graph

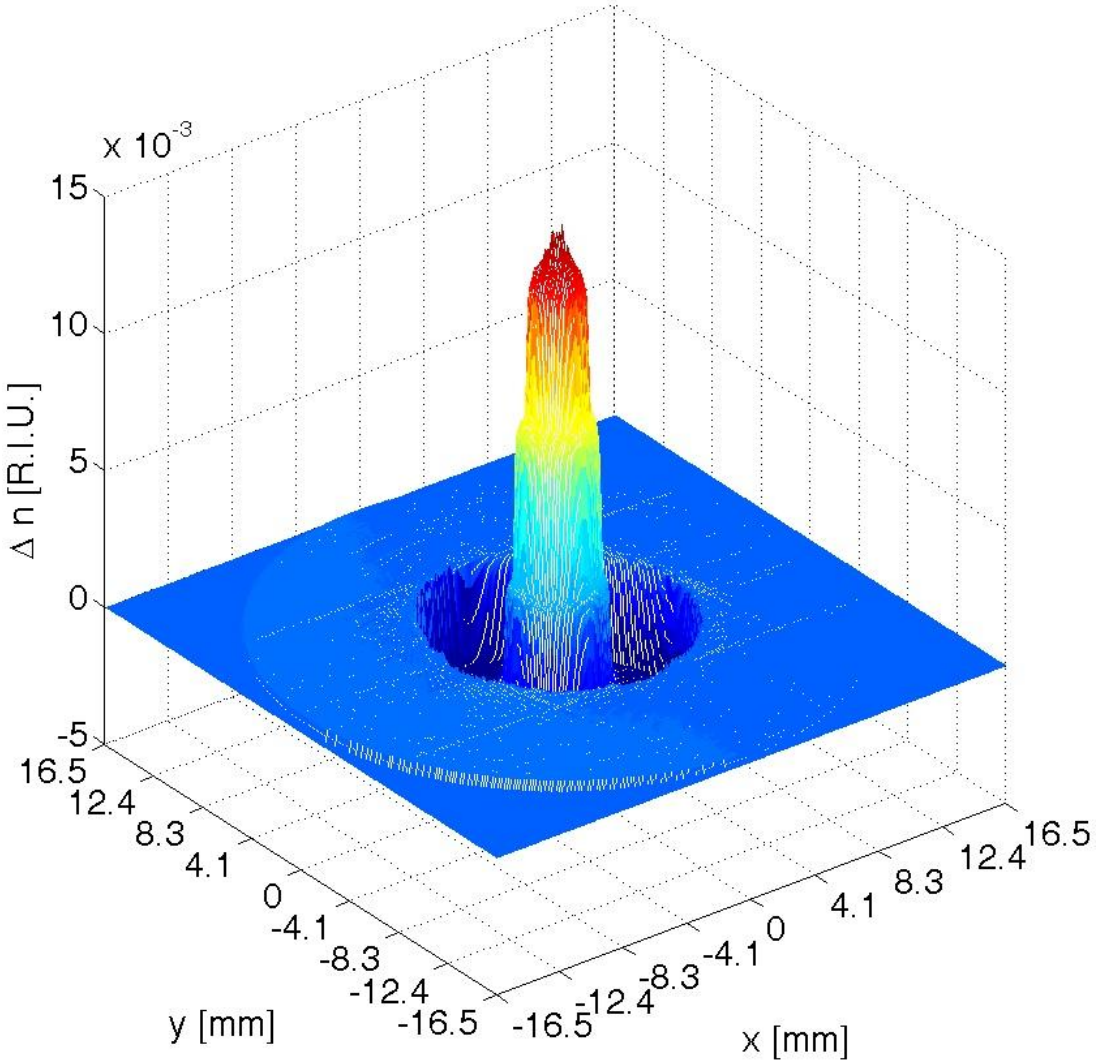

Figure 62 - SG105 in 3D Cartesian coordinates

10.2 Preform SG939: GI+SM

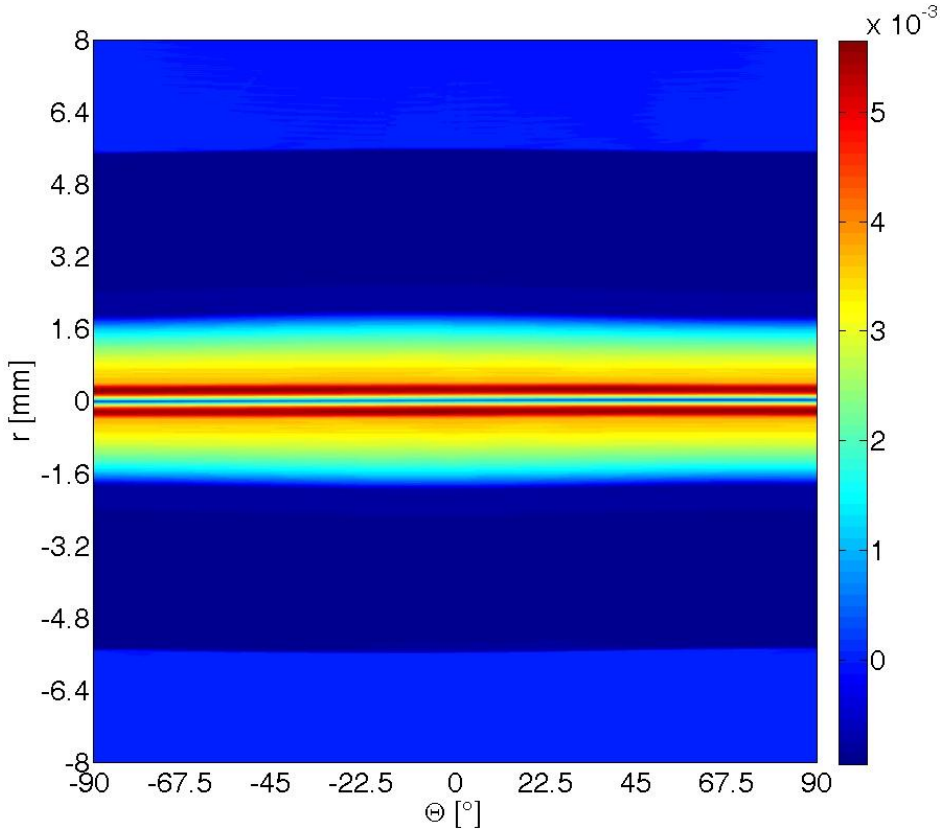

Figure 63 - SG939 in polar coordinates

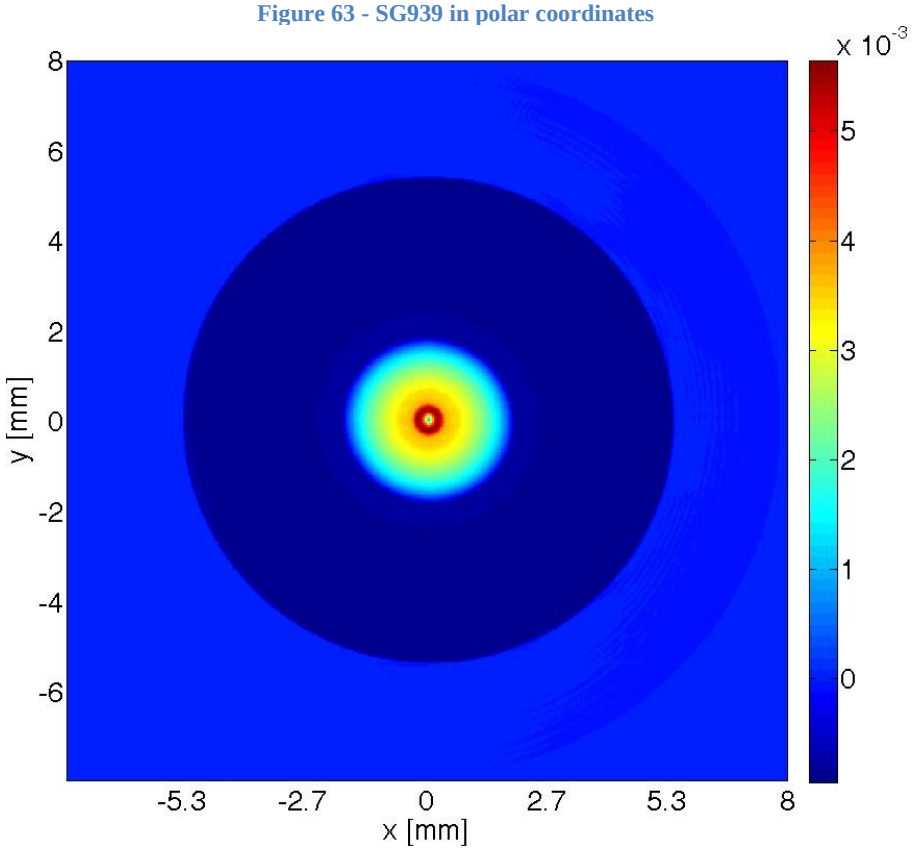

Figure 64 - SG939 Contour graph

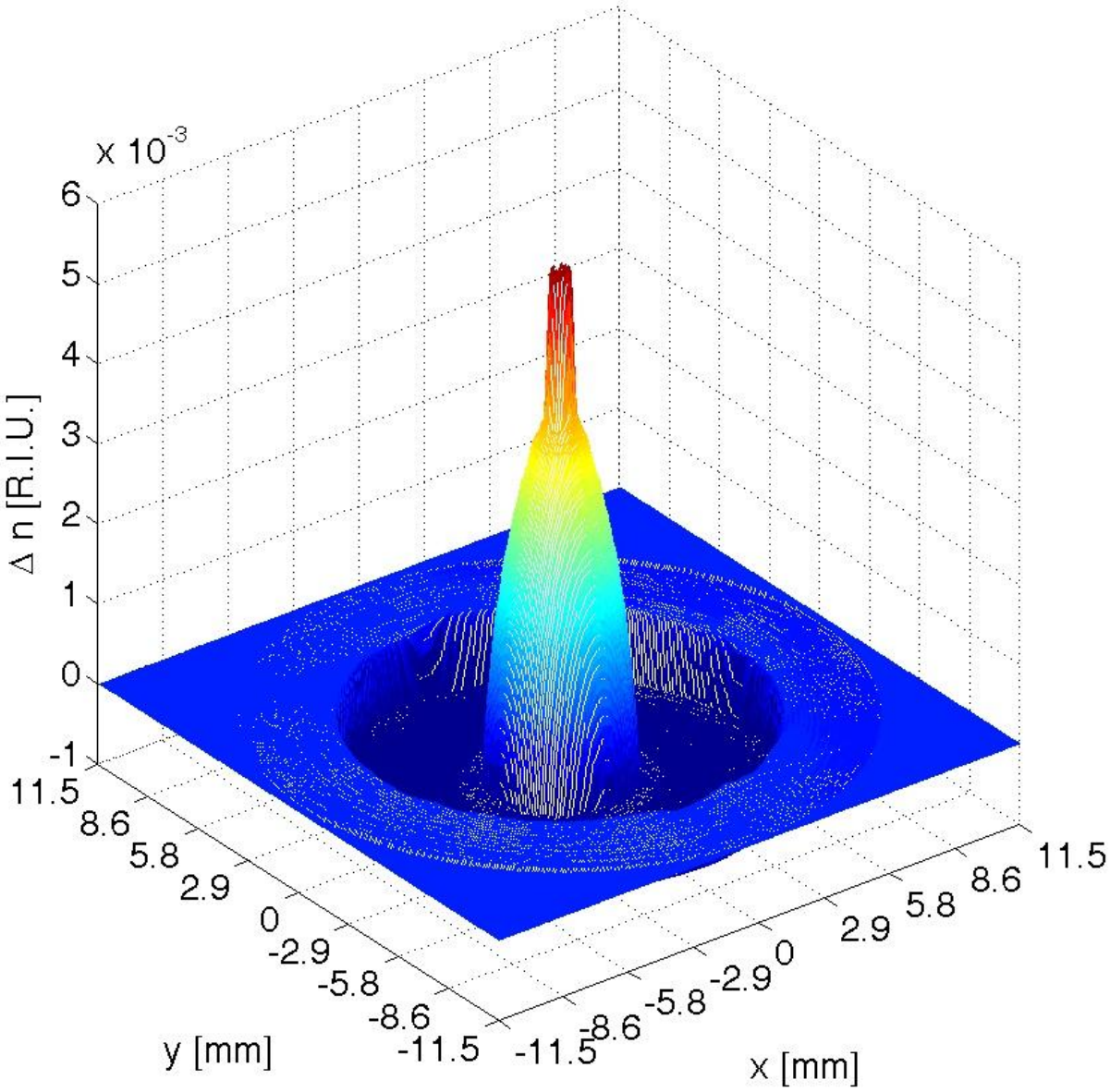

Figure 65 - SG939 in 3D Cartesian coordinates

10.3 Preform SG44: GI + elliptical core

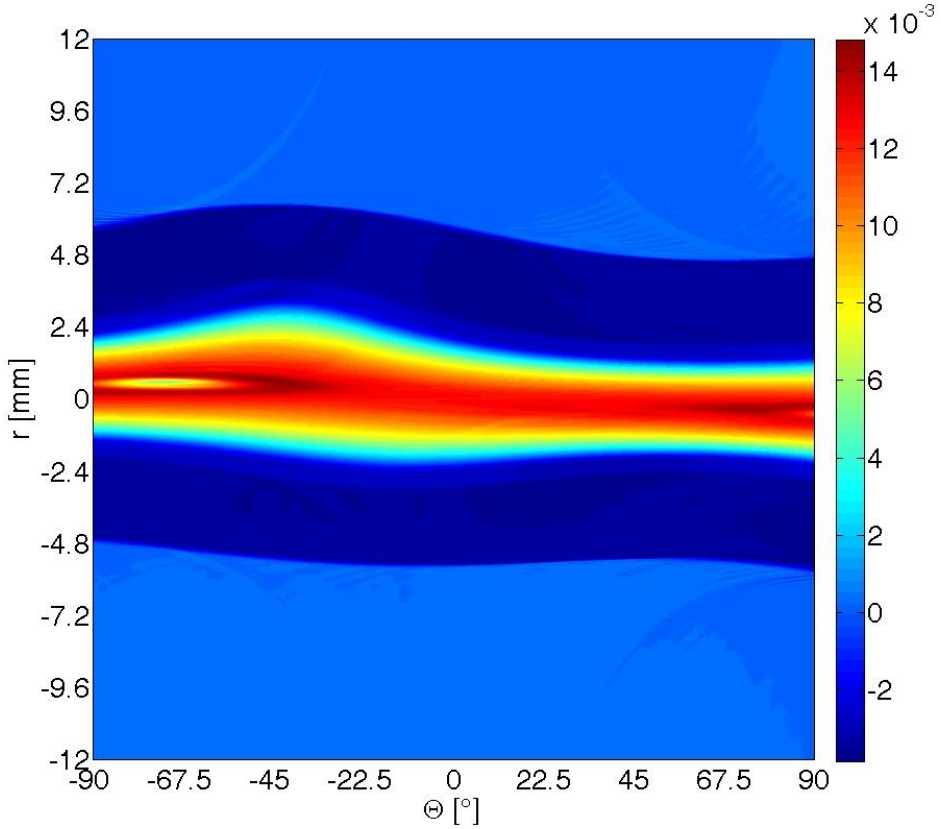

Figure 66 - SG44 in polar coordinates

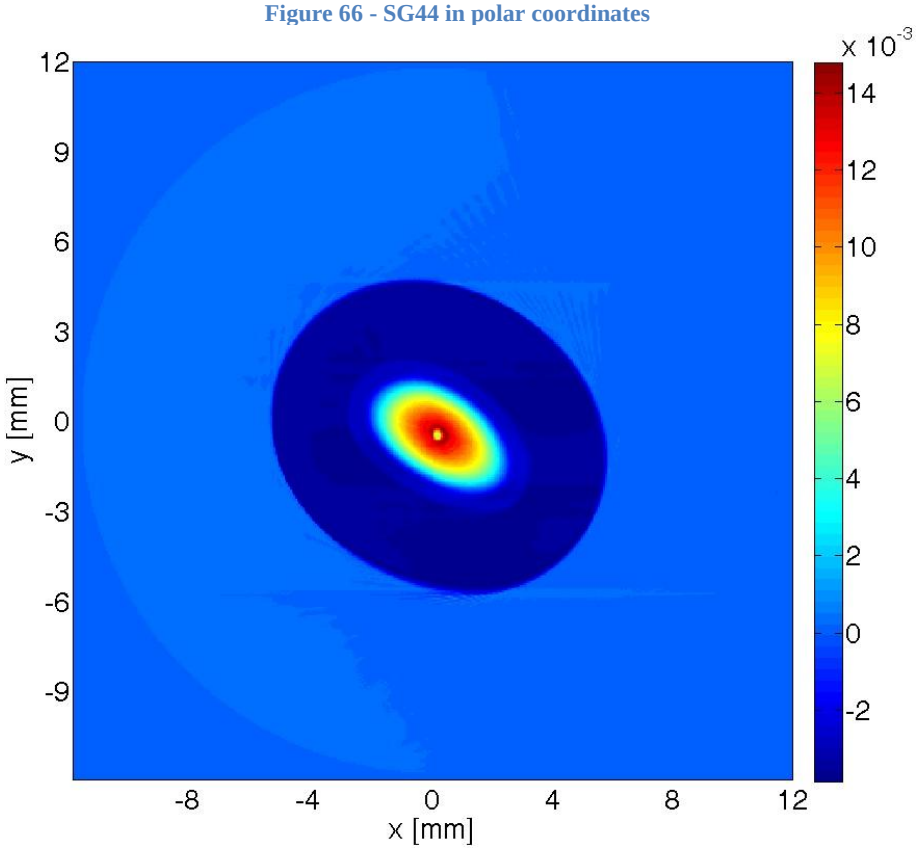

Figure 67 - SG44 Contour graph

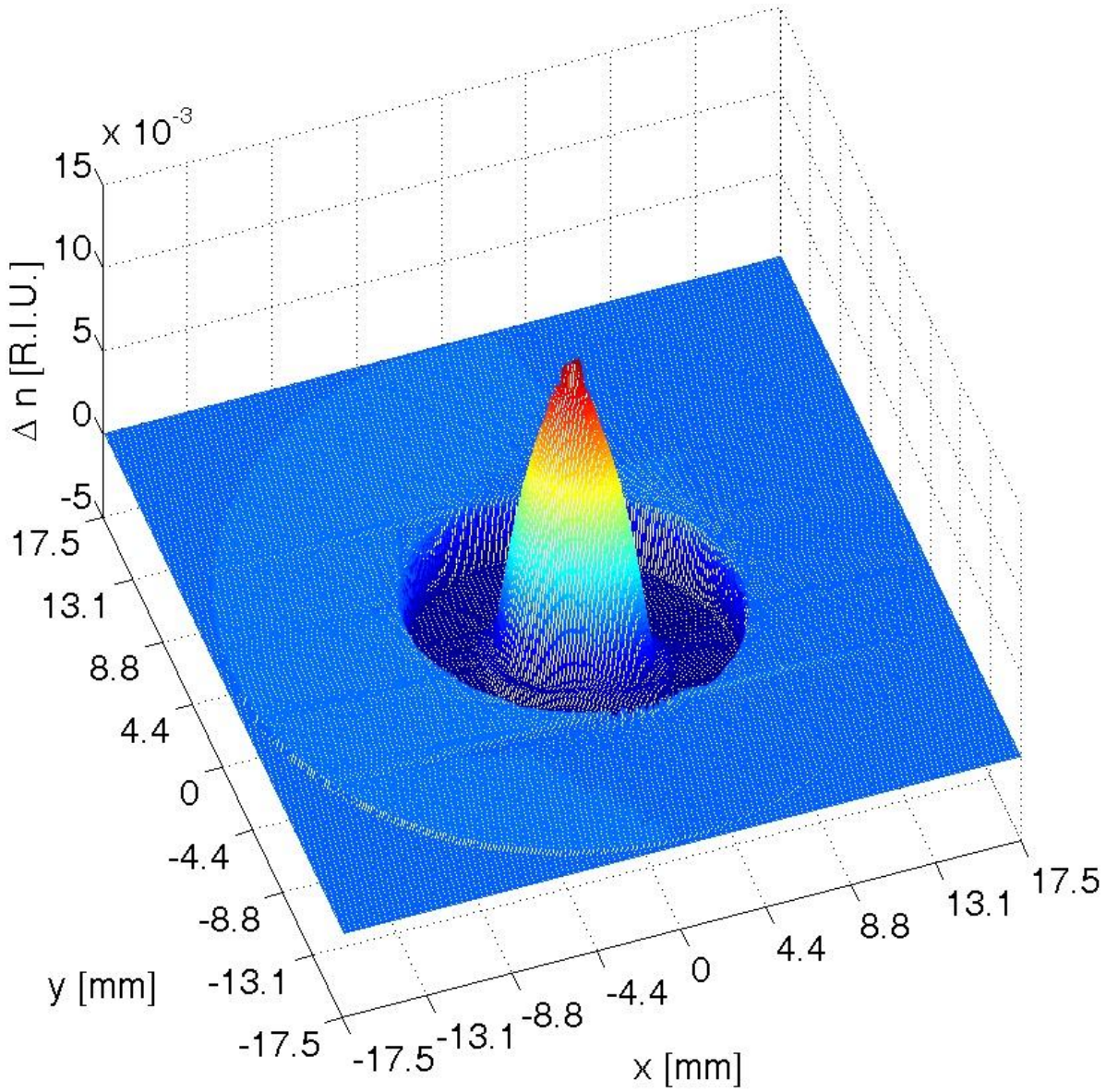

Figure 68 - SG44 in 3D Cartesian coordinates

10.4 Preform SG827:

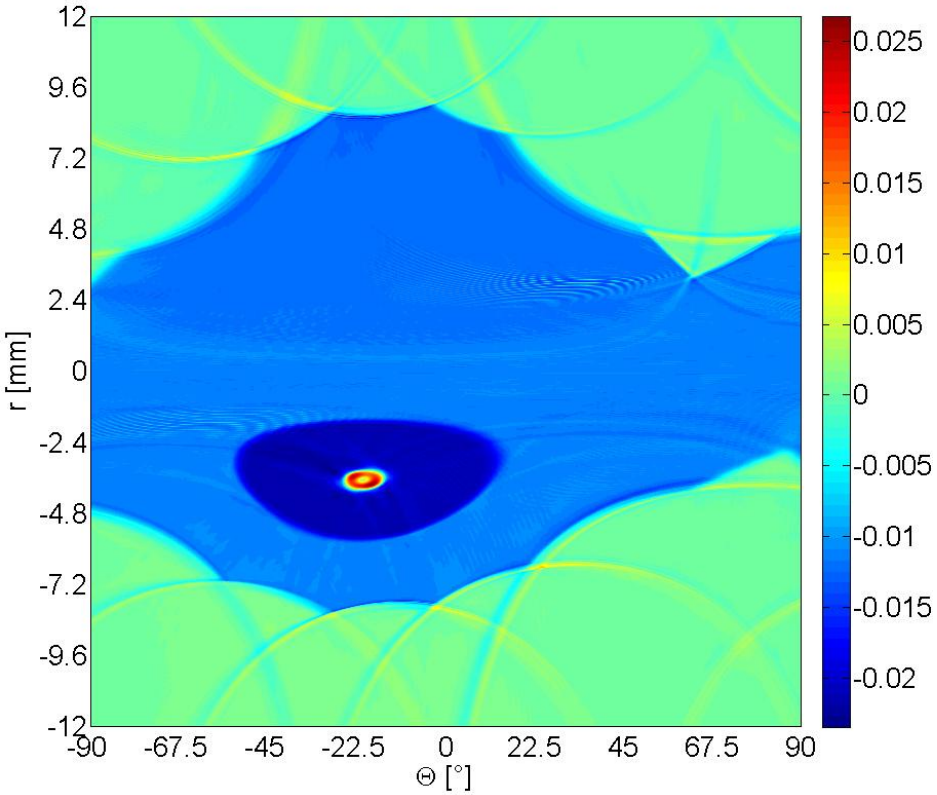

Figure 69 - SG827 in polar coordinates

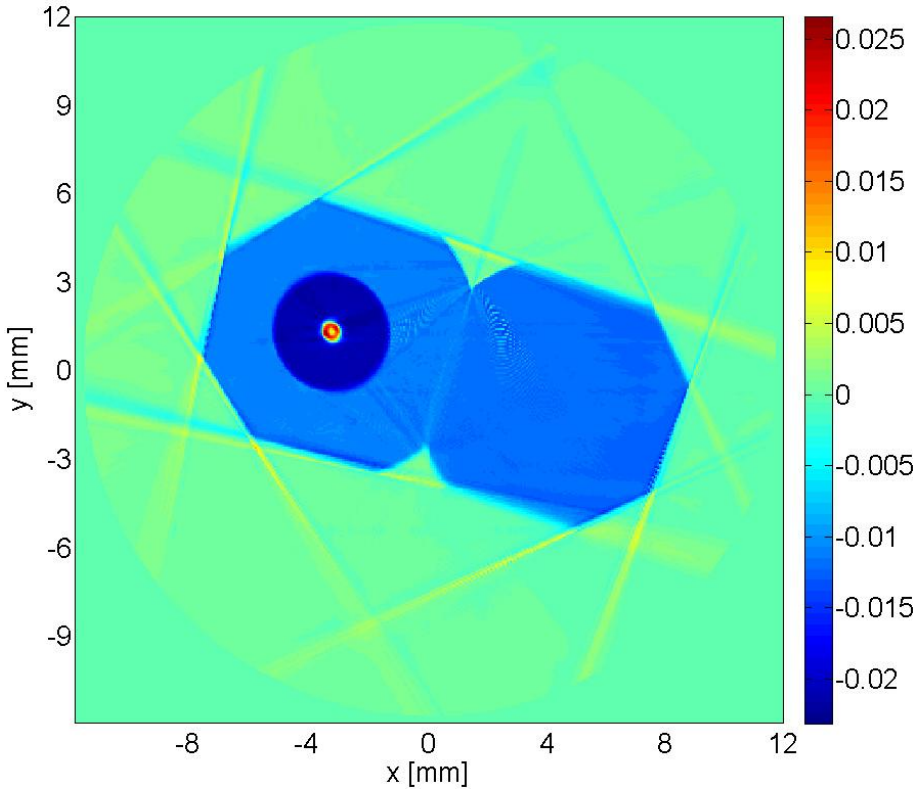

Figure 70 - SG827 Contour graph

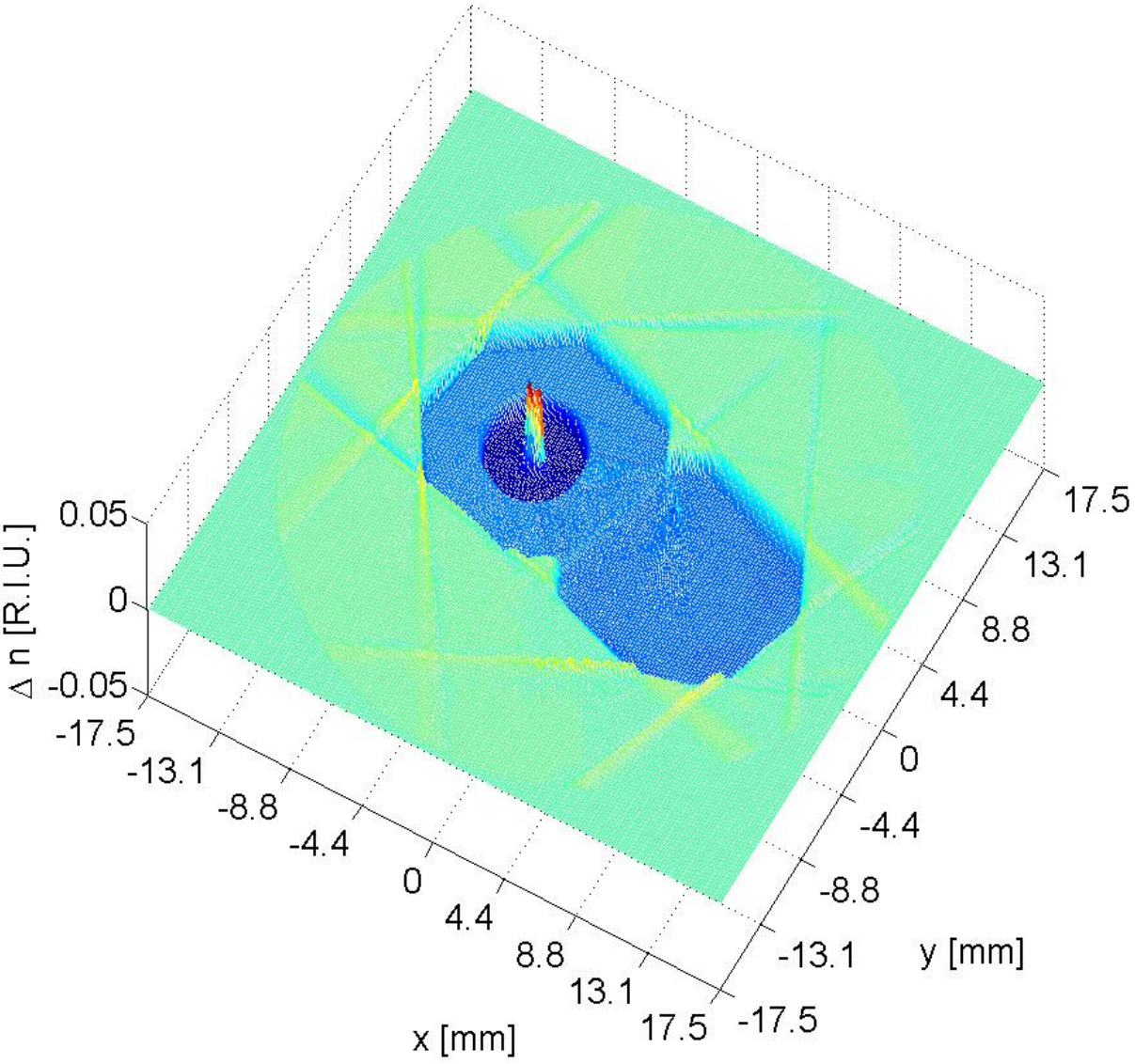

Figure 71 - SG827 in 3D Cartesian coordinates

11 Conclusion

In the previous chapters, we have learned about fibers in general [3] and then about fiber amplifiers and lasers [4]. We have also mentioned the method for end-pumping of double clad optical fiber developed at IPE [4.2.3]. One chapter was devoted to the technique for manufacturing fibers used at the Department of Optical Fibers Technology [4.2.5]. An important part of theoretical work was written about some refractive index profiling methods [5], where we have drawn from the book by Dietrich Marcuse.

In the second half of the work we dealt with the tomographic software, which was the main goal. First, it was necessary to analyze the scripts written by Eng. Jirka Slánička, and then test and modify for our needs [7.1]. Graphical user interface was programmed using the GUIDE as described in the chapter [7.2]. Individual parts of the main program are summarized in paragraph [7.2.1]. It was necessary to translate it into standalone executables, because we want to use Trorip also on workstations, where MATLAB is not installed. This task is discussed in [7.3]. We tested our program Trorip on the theoretical function for the parabolic RIP [8], where the result shows that the program is able reconstruct the RIP very accurately [Figure 48]. In Chapter [9] we have described a brief user's manual. At the end of the thesis we show some examples of measured preforms [10]. The whole thesis is saved in PDF format on CD attached to the thesis book.

With reference to our task [2], we can write that we have fulfilled all the entry points. On the other hand, we expect to have a lot of debugging work, before we would have done this software. I am currently employed at the Institute of Photonics and Electronics, and therefore I am going to continue software development. The results of this thesis we want to present at the 17th Slovak-Czech-Polish Optical Conference, 6 – 10 September 2010 in Liptovský Ján, Slovakia.

12 References

12.1 Documents

[D1] BAILEY, David. WRIGHT, Edwin. *Practical Fiber Optics.* 1st edition. NEWNES. Great Britain 2003. ISBN 978-0-7506-5800-3.

[D2] LEE, T. P. *Current Trends in Optical Amplifiers and Their Applications*. World Scientific Publishing. Singapore 1996. ISBN 981-02-2695-0.

[D3] SNITZER, Elias. *Amplification in a fiber laser*. Applied Optics. 1182-1186. 1964.

[D4] PETERKA, P. HONZATKO, P. KARÁSEK, M. KAŇKA, J. KAŠÍK, I. MAŤEJEC, V. *Vláknové lasery – princip a aplikace*. Jemná Mechanika a Optika. 4/2010, vol. 55, Page 115-120. ISSN 0447-6441.

[D5] PETERKA, P. KASIK, I. MATEJEC, V. KARASEK, M. KANKA, J. HONZATKO, P. KUBECEK, V. *Amplifier Performance of Double-Clad Er/Yb-Doped Fiber with Cross-Section Tailored for Direct Splicing to the Pump and Signal Fibers.* Optical Fiber Communication and the National Fiber Optic Engineers Conference. Anaheim, CA 25-29 March 2007. ISBN: 1-55752-831-4. INSPEC Accession Number: 9695523.

[D6] AGRAWAL, Govind P. *Applications of nonlinear fiber optics*. Academic Press. San Diego 2001. ISBN 0-12-045144-1.

[D7] KAWAI, Shigeru. *Handbook of Optical Interconnects*. CRC Press. USA 2005. ISBN 978-0-8247-2441-2.

[D8] DIETRICH, Marcuse. *Principles of Optical Fiber Measurements*. Academic Press. USA 1981. ISBN 0-12-470980-X.

[D9] DAI, Xinhua. AI, Xicheng. LIU, Zhimin. YANG, Mingjun. YANG, Guangying. HAN, Buxing. XU, Jian. ZHANG, Xianmin. WU, Xin. *Characterization of refractive index distribution of polymer optical fiber*. Chinese Science Bulletin Vol. 47 No. 12. China June 2002.

[D10] Photon Kinetics, Inc. *2600 PREFORM ANALYZER USER'S MANUAL*. USA 2004.

[D11] CHU, P, L. WHITBREAD, T. *Nondestructive determination of refractive index profile of an optical fiber: fast Fourier transfor7m method.* Applied Optics. Page 1117-1122. Vol. 18. No. 7. April 1979.

[D12] ZHAO, Yucheng. FLEMING, Simon. LYYTIKAINEN, Katja. POLADIAN, Leon. *Nondestructive Measurement for Arbitrary RIP Distribution of Optical Fiber Preforms*. Journal of lightwave technology. Page 478-486. Vol. 22. No. 2. February 2004.

[D13] SLÁNIČKA, Jiří. PETERKA, Pavel. MATĚJEC, Vlastimil. KAŠÍK, Ivan. POSPÍŠILOVÁ, Marie. *Tomografická rekonstrukce geometrie a profilu indexu lomu preforem speciálních optických vláken*. Conference Optické Komunikace 2005. Page 121-127. Prague October 2005.

[D14] SLÁNIČKA, Jiří. *Tomografická rekonstrukce profilu indexu lomu preforem speciálních optických vláken*. ČVUT-FEL, Katedra radioelektroniky. Prague 2007.

12.2 Software

[S1] MATLAB 7.1, c1984 – 2005 The MathWorks
URL: < http://www.humusoft.cz/produkty/matlab >

[S2] 2600 Preform Analyzer software; sav2txt.exe – c2004 Photon Kinetics
URL: < http://www.pkinetics.com/ >

12.3 WWW sources

[W1] Institute of Photonics and Electronics
URL: < http:// http://www.ufe.cz/ >

[W2] Wikipedia – The Free Encyclopedia
URL: < http://en.wikipedia.org >

[W3] Jeff Hecht – A Fiber-Optic Chronology
URL: < http://www.sff.net/people/Jeff.Hecht/Chron.html >

[W4] Encyclopedia of Laser Physics and Technology
URL: < http://www.rp-photonics.com >

[W5] Dictionary, Encyclopedia and Thesaurus - The Free Dictionary
URL: < http://encyclopedia.thefreedictionary.com >

[W6] MathWorks - MATLAB and Simulink for Technical Computing
URL: < http://www.mathworks.com/ >

[W7] The MathWorks - Bug Reports
URL: < http://www.mathworks.com/support/bugreports/531531 >